Nanomaterials

- Metals and Alloys
  - Fe, Al, Au
- Semiconductors
  - Band gap, CdS, TiO_2, ZnO
- Ceramic
  - Al_2O_3, Si_3N_4, MgO, , SiO_2, ZrO_2
- Carbon based
  - Diamond, graphite, nanotube, C60, graphene
- Polymers
  - Soft mater, block co-polymer
- Biological
  - Photonic, hydrophobic, adhesive,
- Composites

Surface to Volume Ratio

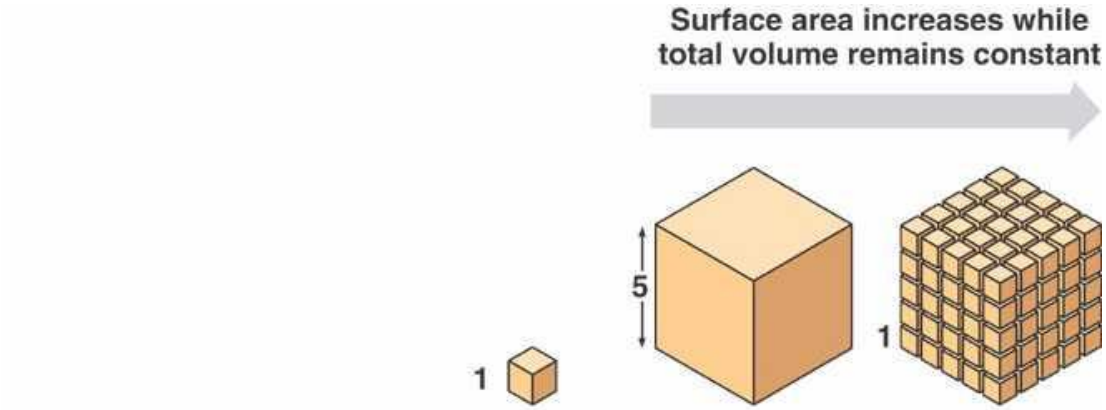

Total surface area (height × width × number of sides × number of boxes)	6	150	750
Total volume (height × width × length × number of boxes)	1	125	125
Surface-to-volume ratio (surface area / volume)	6	1.2	6

Surface Energy

One face surface energy: γ
27 cube: 27 x 6 γ
3 x 9 cube line: 114 γ
3 x (3x3) square: 90 γ
3 x 3 x 3 cube: 54 γ

Surface to Volume Ratio

Au: AAA
Atomic mass: 196.967
Density 19.31
Radii =0.144 nm

Number of Au atoms in 1 m	$3.4\ 10^{9}$
Volume of Au atom	$4.19\ 10^{28}$
Surface area Au atom	$7.22\ 10^{19}$
Surface/volume ratio	$1.72\ 10^{-9}$

fcc

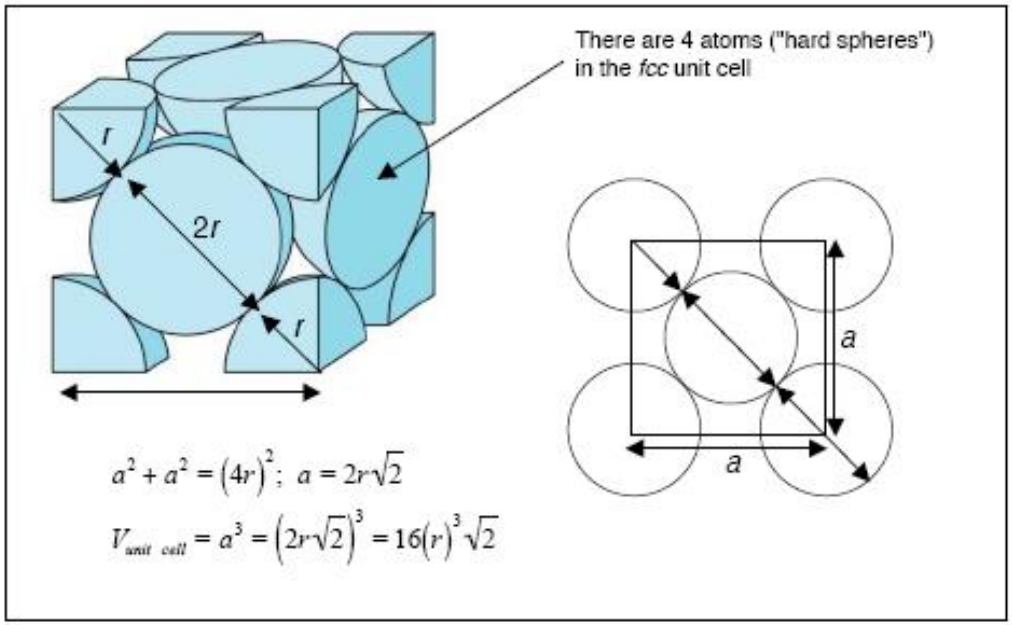

$V_{unit\ cell} = a^3 = (2r\sqrt{2})^3 = 16(0.5\text{nm})^3\sqrt{2} = \mathbf{2.828\ nm^3}$

$\frac{10^{27}\ \text{nm}^3}{2.828\ \text{nm}^3} = \mathbf{3.536x10^{26}\ nano\ unit\ cells}$

$\frac{S_{spheres}}{S_{unit\ cell}} = \frac{4.44x10^9\ \text{m}^2}{6.0x10^9\ \text{m}^2} = \mathbf{0.74}$

Collective Area = $3.536x10^{26}$ nano unit cells $\left(\frac{4\ \text{spheres}}{\text{unit cell}}\right)\left(\frac{4\pi r^2}{\text{sphere}}\right) = \mathbf{4.44x10^{27}\ nm^2}$

Packing Fraction

$$\mathrm{APF} = \frac{N_{\mathrm{atoms}} V_{\mathrm{atom}}}{V_{\mathrm{crystal}}}$$

Surfaces

- Collective surface area of nanocube 1 nm
- Porous materials
  - Micropore (<2 nm)
  - Mesopore (2 nm ~ 50 nm)
  - Marcopore (> 50nm)
- Void volume
  - $V_{pore}/V_{material}$

Bandgap

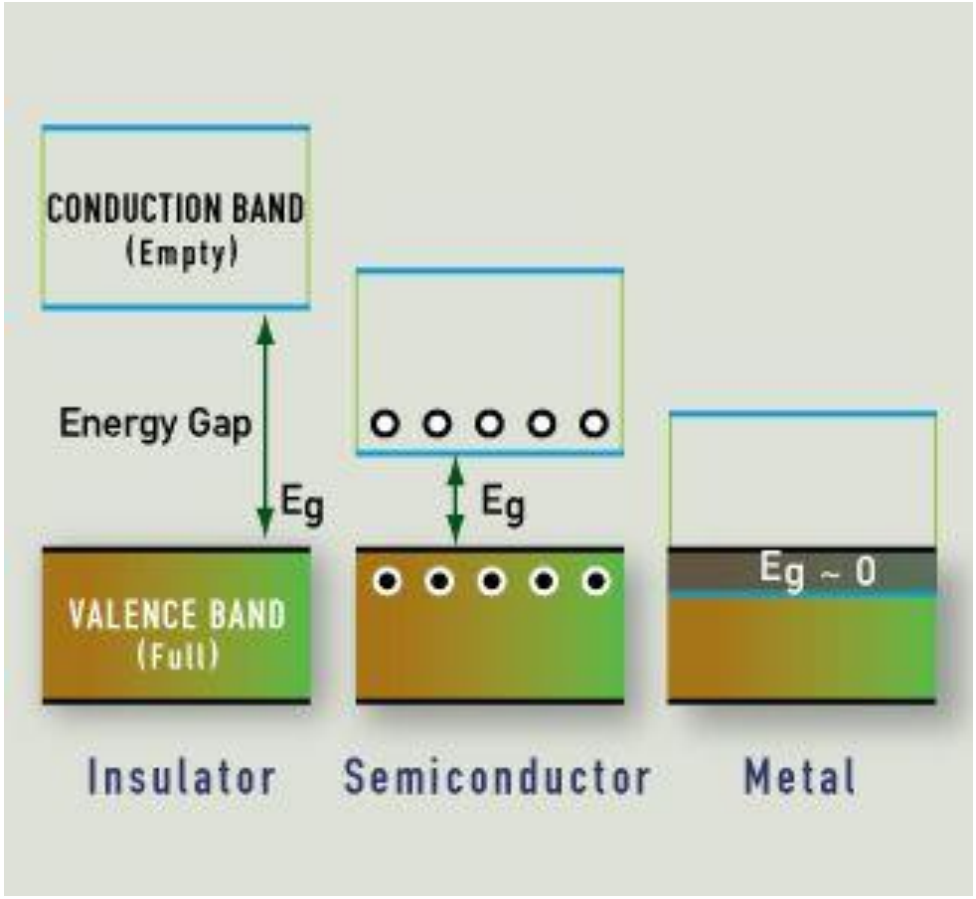
CONDUCTION BAND
(Empty)
Energy Gap
Eg
VALENCE BAND
(Full)
Eg
Eg ~ 0
Insulator
Semiconductor
Metal

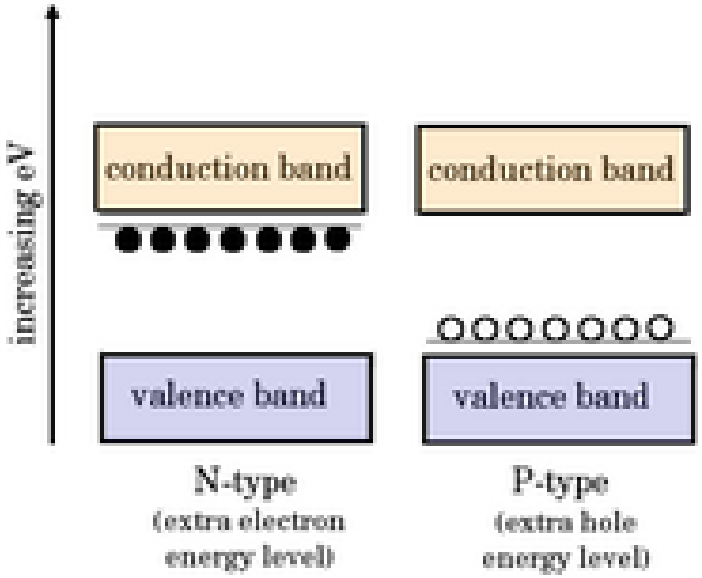
increasing eV
conduction band
conduction band
valence band
valence band
N-type
(extra electron
energy level)
P-type
(extra hole
energy level)

Bandgap

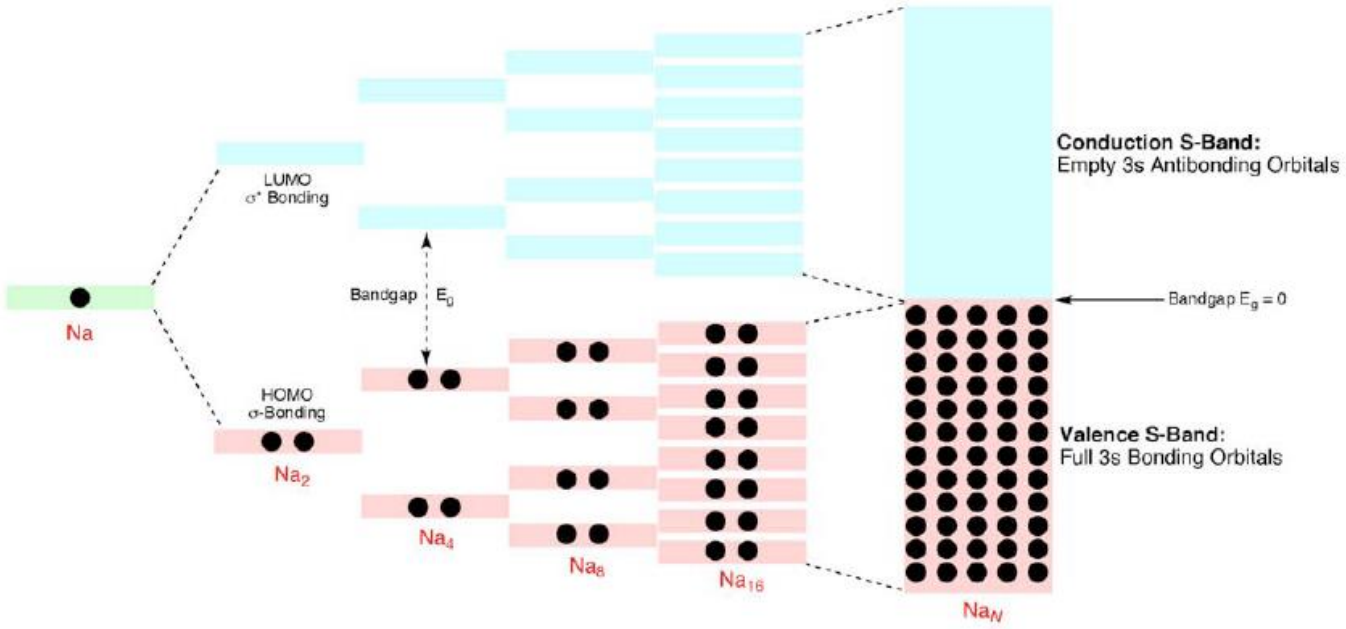
LUMO
σ* Bonding
HOMO
σ-Bonding
Na
Na2
Na4
Na8
Na16
NaN
Bandgap E0
Conduction S-Band:
Empty 3s Antibonding Orbitals
Bandgap Eg = 0
Valence S-Band:
Full 3s Bonding Orbitals

Particle in a Box

$$-\frac{\hbar^2}{2m}\frac{\mathrm{d}^2\psi(x)}{\mathrm{d}x^2} + V(x)\psi(x) = E\psi(x) \quad (1)$$

$$\psi_n = \sqrt{\frac{2}{L}}\sin\left(\frac{n\pi x}{L}\right)$$

$$E_n = \frac{\hbar^2\pi^2}{2mL^2}n^2$$

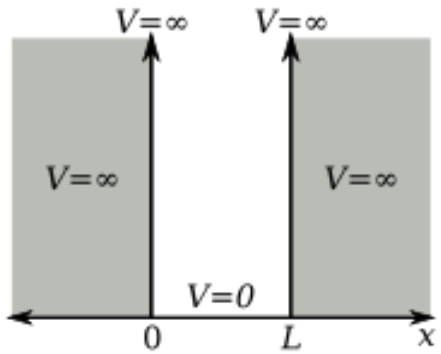

Particle in a Box

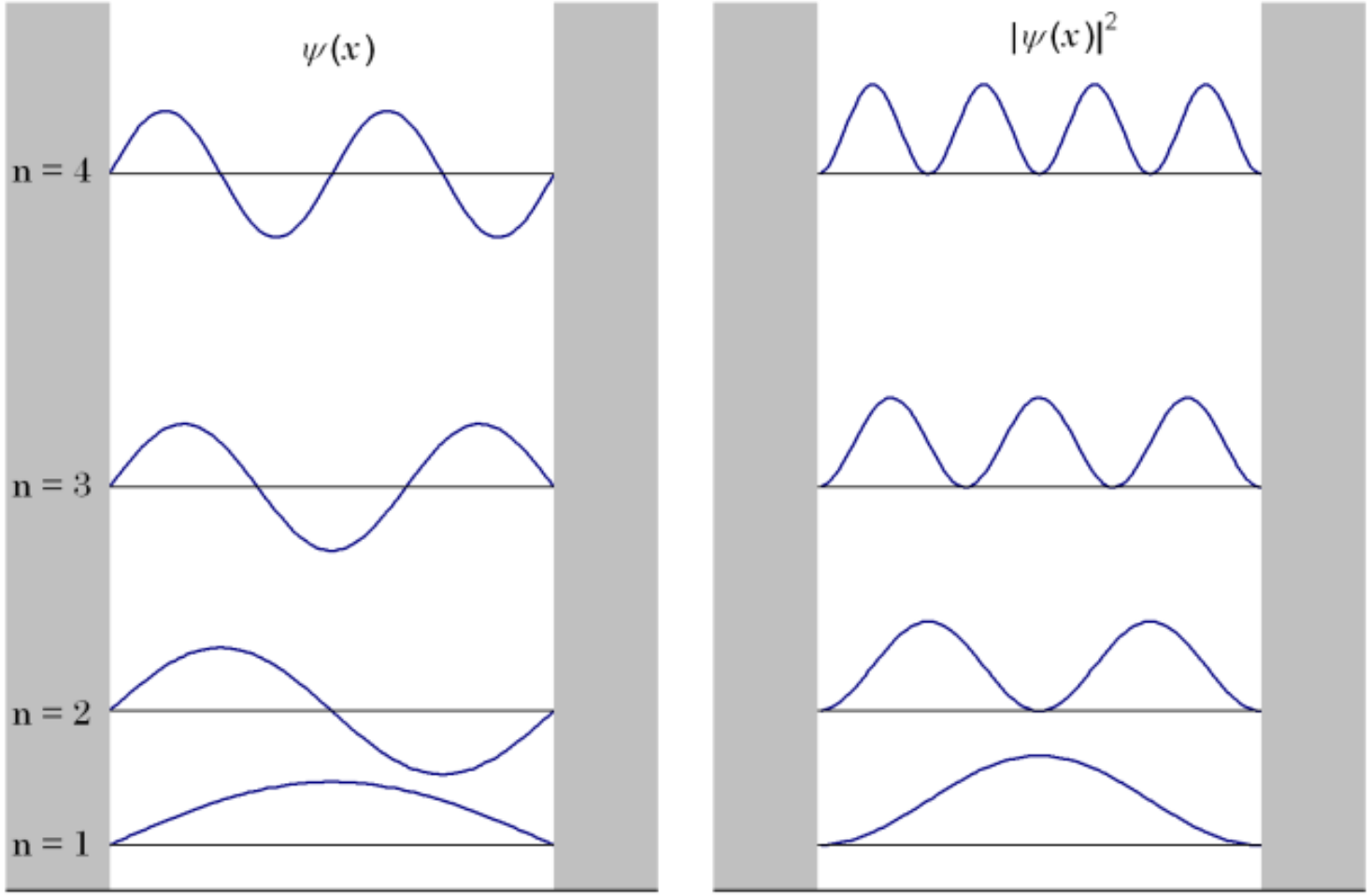

$$\psi_{n_x,n_y} = \sqrt{\frac{4}{L_x L_y}} \sin\left(\frac{n_x \pi x}{L_x}\right) \sin\left(\frac{n_y \pi y}{L_y}\right)$$

$$E_{n_x,n_y} = \frac{\hbar^2 \pi^2}{2m} \left[\left(\frac{n_x}{L_x}\right)^2 + \left(\frac{n_y}{L_y}\right)^2\right]$$

$$\psi_{n_x,n_y,n_z} = \sqrt{\frac{8}{L_x L_y L_z}} \sin\left(\frac{n_x \pi x}{L_x}\right) \sin\left(\frac{n_y \pi y}{L_y}\right) \sin\left(\frac{n_z \pi z}{L_z}\right) \quad (22)$$

$$E_{n_x,n_y,n_z} = \frac{\hbar^2 \pi^2}{2m} \left[\left(\frac{n_x}{L_x}\right)^2 + \left(\frac{n_y}{L_y}\right)^2 + \left(\frac{n_z}{L_z}\right)^2\right] \quad (23)$$

Wave Functions

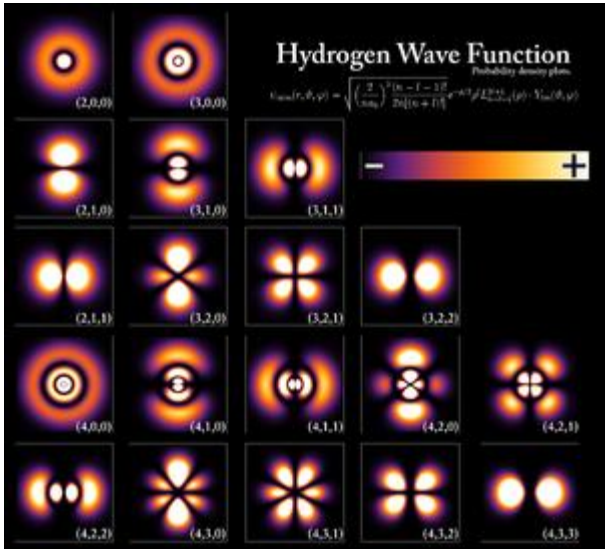

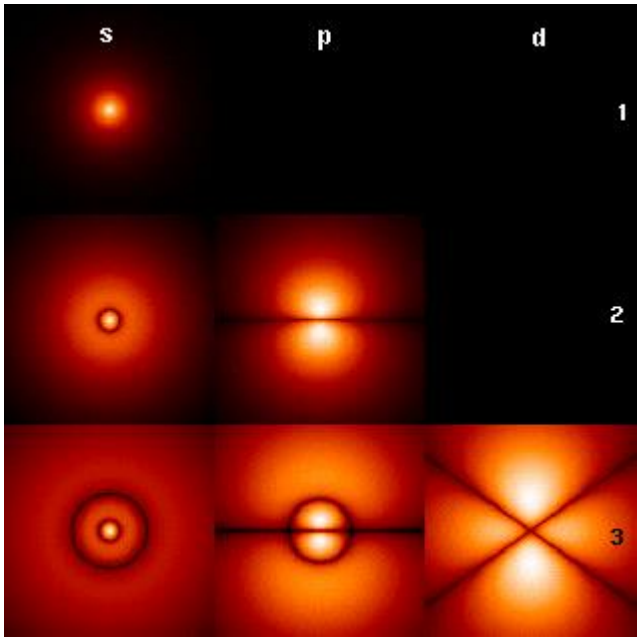

$$i\hbar\frac{\partial}{\partial t}\Psi(\mathbf{r},\,t) = \hat{H}\Psi = \left(-\frac{\hbar^2}{2m}\nabla^2 + V(\mathbf{r})\right)\Psi(\mathbf{r},\,t) = -\frac{\hbar^2}{2m}\nabla^2\Psi(\mathbf{r},\,t) + V(\mathbf{r})\Psi(\mathbf{r},\,t)$$

$$V(r) = -\frac{1}{4\pi\epsilon_0}\frac{Ze^2}{r}$$

$$\psi_{n\ell m}(r,\vartheta,\varphi) = \sqrt{\left(\frac{2}{na_0}\right)^3\frac{(n-\ell-1)!}{2n(n+\ell)!}}e^{-\rho/2}\rho^\ell L_{n-\ell-1}^{2\ell+1}(\rho)\cdot Y_\ell^m(\vartheta,\varphi)$$

Linear combination of atomic orbitals molecular orbital method

$$\phi_i = c_{1i}\chi_1 + c_{2i}\chi_2 + c_{3i}\chi_3 + \cdots + c_{ni}\chi_n$$

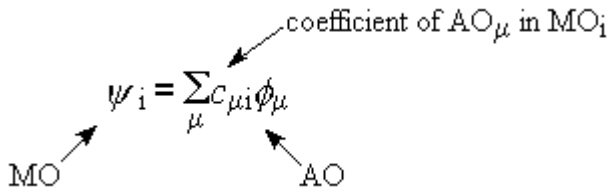

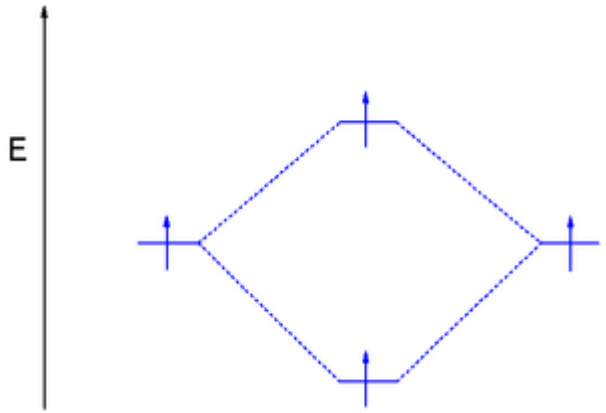

Oxygen

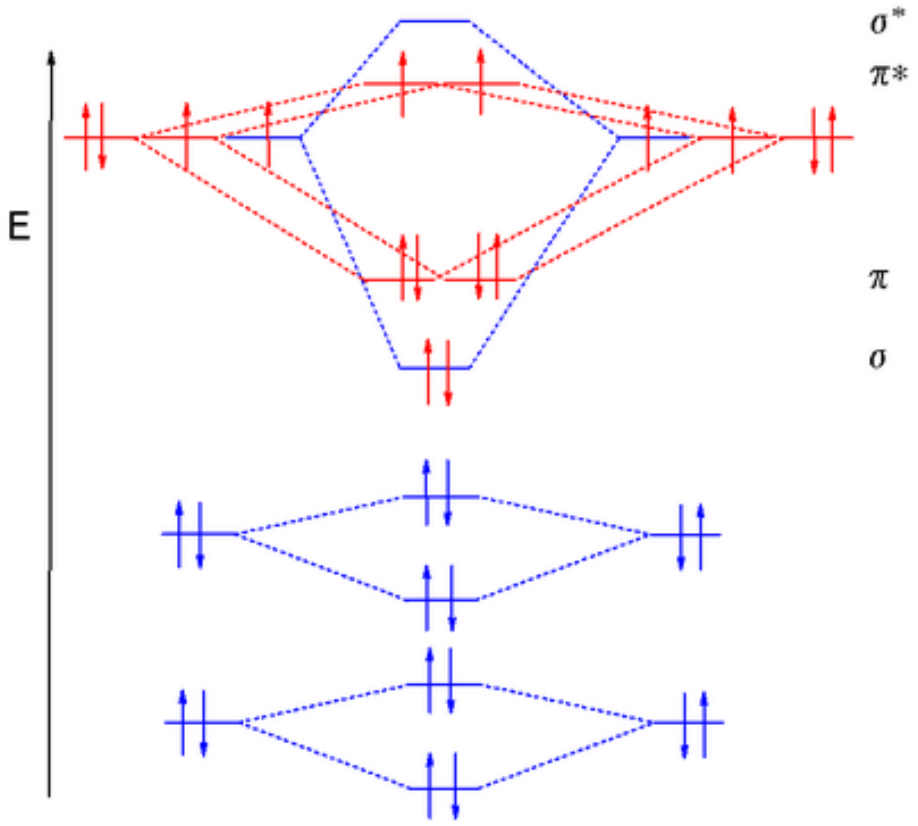

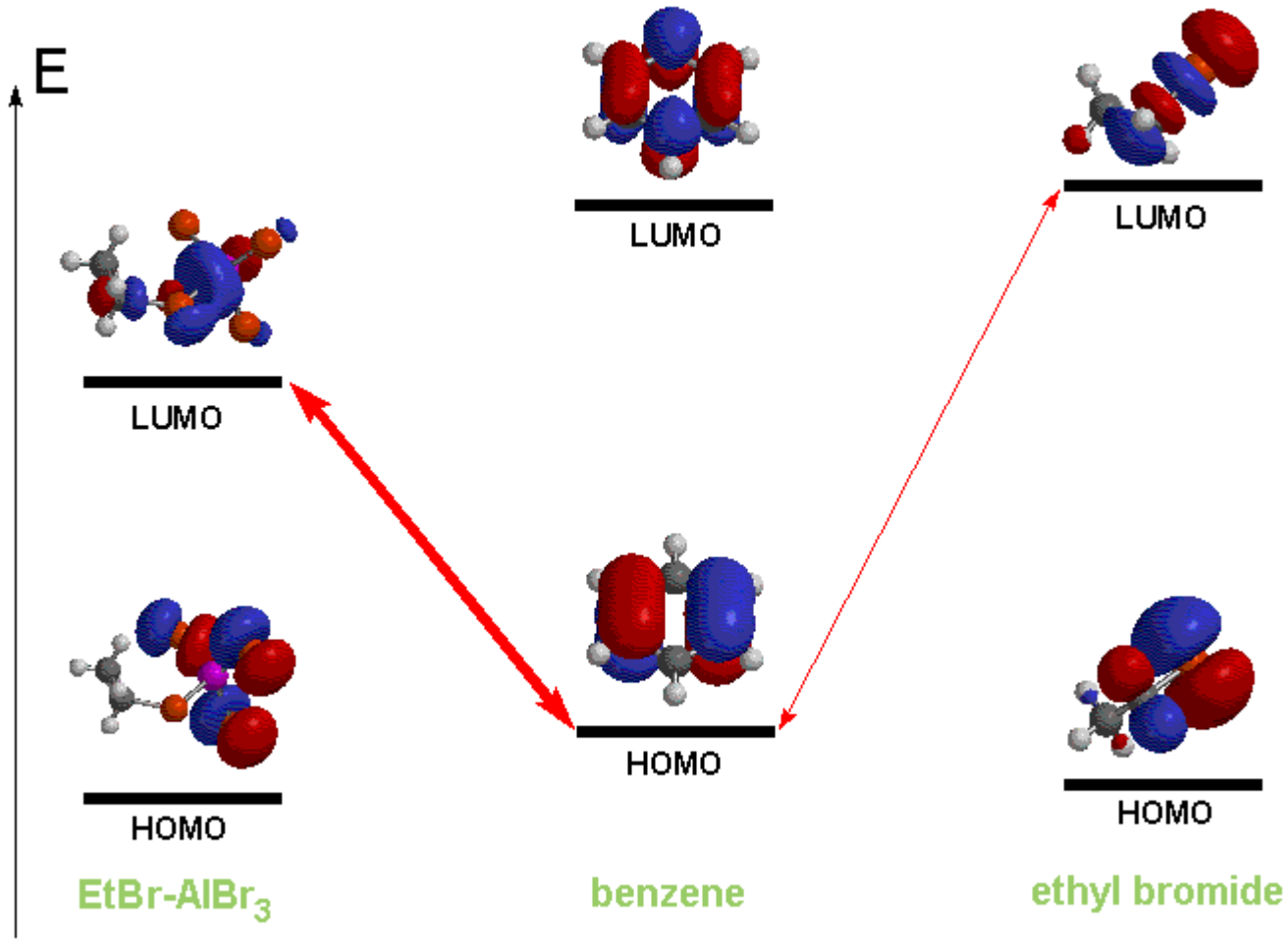
E
LUMO
HOMO
LUMO
HOMO
LUMO
HOMO
EtBr-AlBr3
benzene
ethyl bromide

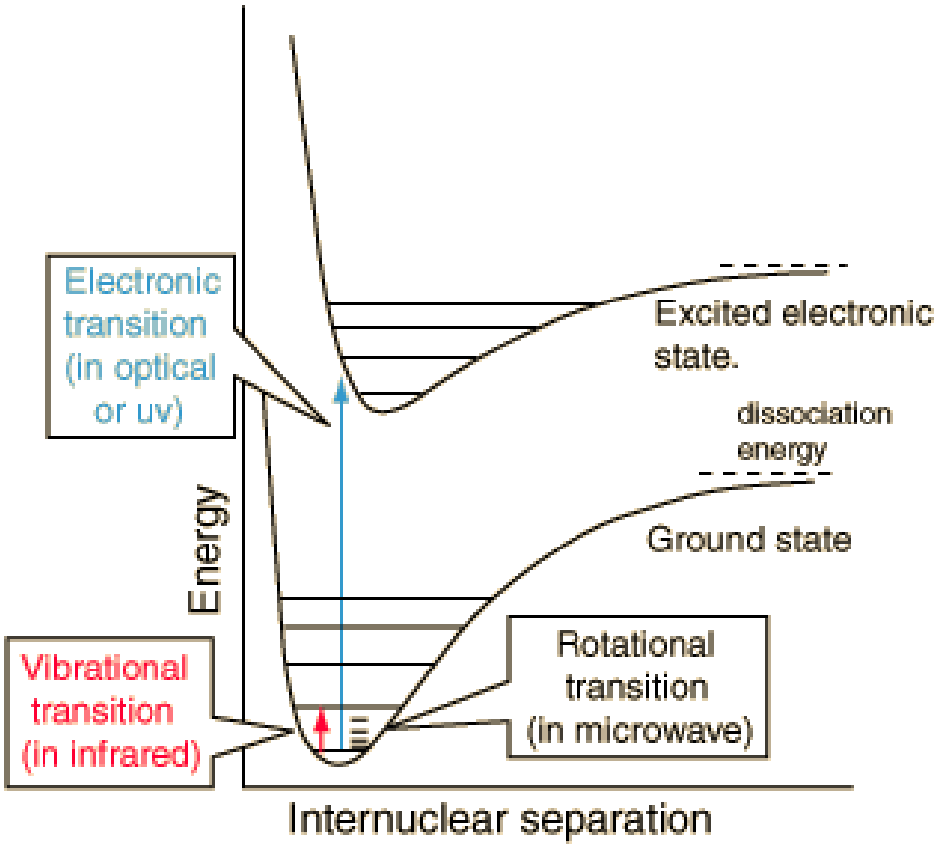
Electronic transition (in optical or uv)
Excited electronic state.
dissociation energy
Ground state
Energy
Vibrational transition (in infrared)
Rotational transition (in microwave)
Internuclear separation

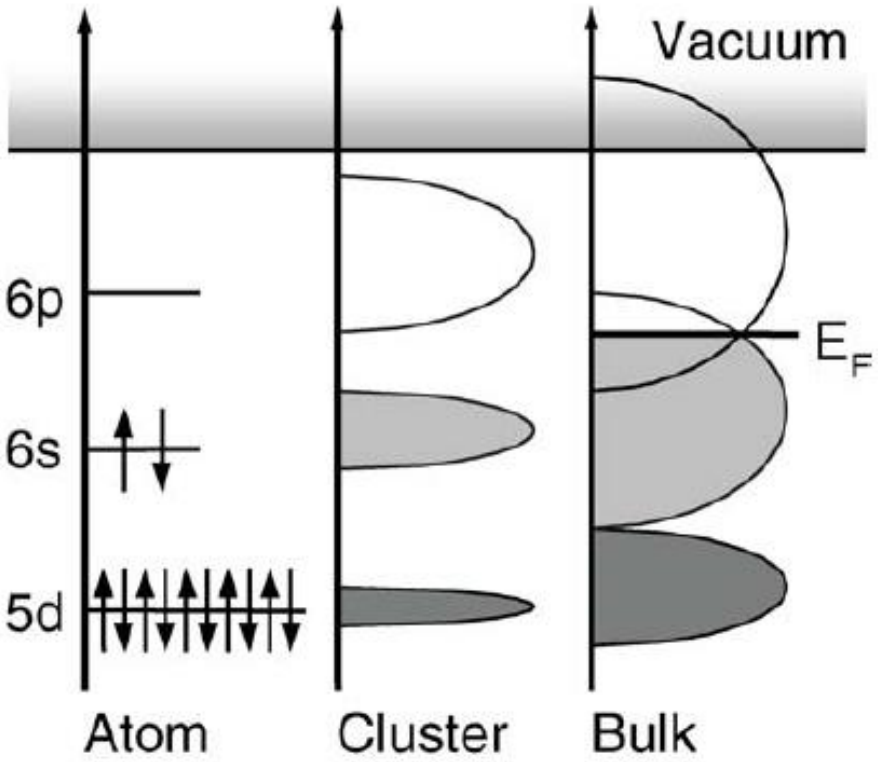

Figure 5 Energy diagram describing a generic Bloch-Wilson MIT in clusters (with specific reference to the energy levels of mercury). For sufficiently large clusters, the *s-p* band gap closes with increasing cluster size (shaded areas represent energy range with occupied electron levels). Overlap leads to a "continuous" DOS at E_F and to an Insulator to Metal transition.

Bloch wave

$$\psi_{n\mathbf{k}}(\mathbf{r}) = e^{i\mathbf{k}\cdot\mathbf{r}} u_{n\mathbf{k}}(\mathbf{r})$$

A **Bloch wave** or **Bloch state**, named after Felix Bloch, is the wavefunction of a particle (usually, an electron) placed in a periodic potential.

$\epsilon n(\mathbf{k}) = \epsilon n(\mathbf{k} + \mathbf{K})$,

The five fundamental two-dimensional Bravais lattices

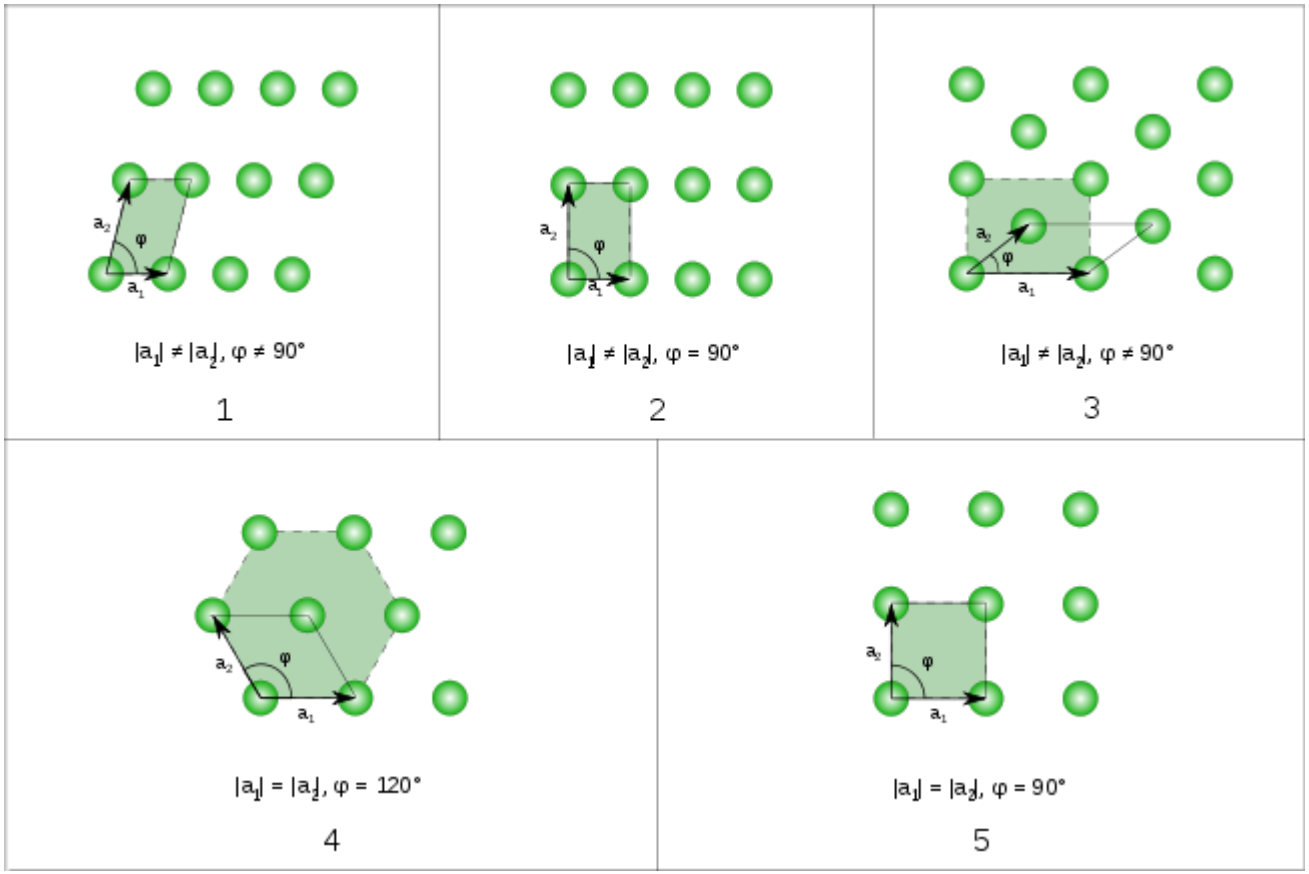

Unit Cell

Bravais lattice	Parameters	Simple (P)	Volume centered (I)	Base centered (C)	Face centered (F)
Triclinic	$a_1 \neq a_2 \neq a_3$ $\alpha_{12} \neq \alpha_{23} \neq \alpha_{31}$	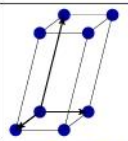			
Monoclinic	$a_1 \neq a_2 \neq a_3$ $\alpha_{23} = \alpha_{31} = 90°$ $\alpha_{12} \neq 90°$	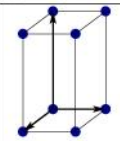	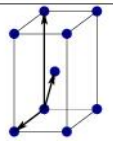		
Orthorhombic	$a_1 \neq a_2 \neq a_3$ $\alpha_{12} = \alpha_{23} = \alpha_{31} = 90°$	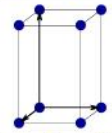	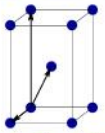	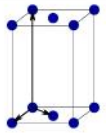	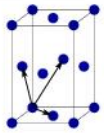
Tetragonal	$a_1 = a_2 \neq a_3$ $\alpha_{12} = \alpha_{23} = \alpha_{31} = 90°$	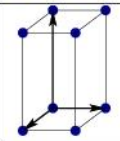	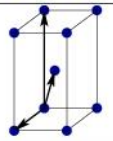		
Trigonal	$a_1 = a_2 = a_3$ $\alpha_{12} = \alpha_{23} = \alpha_{31} < 120°$				
Cubic	$a_1 = a_2 = a_3$ $\alpha_{12} = \alpha_{23} = \alpha_{31} = 90°$	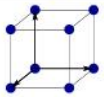			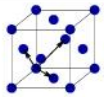
Hexagonal	$a_1 = a_2 \neq a_3$ $\alpha_{12} = 120°$ $\alpha_{23} = \alpha_{31} = 90°$	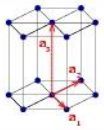			

Table 1.1: Bravais lattices in three-dimensions.

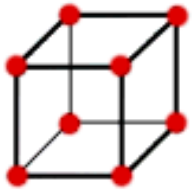

Simple cubic

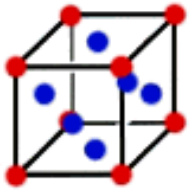

Face-centered cubic

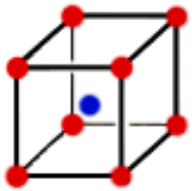

Body-centered cubic

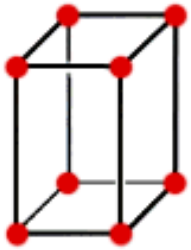

Simple tetragonal

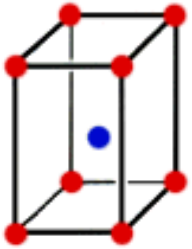

Body-centered tetragonal

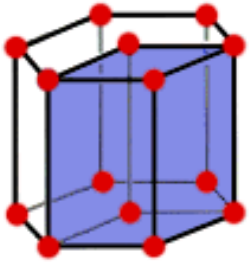

Hexagonal

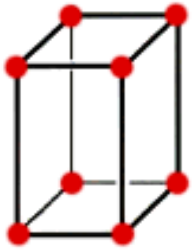

Simple orthorhombic

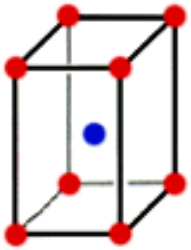

Body-centered orthorhombic

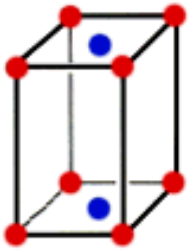

Base-centered orthorhombic

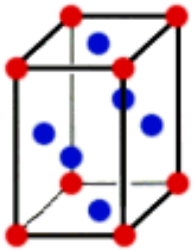

Face-centered orthorhombic

Rhombohedral

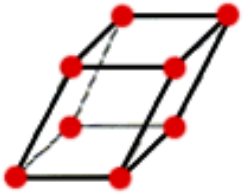

Simple Monoclinic

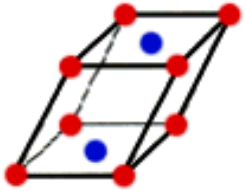

Base-centered monoclinic

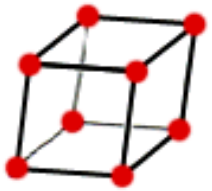

Triclinic

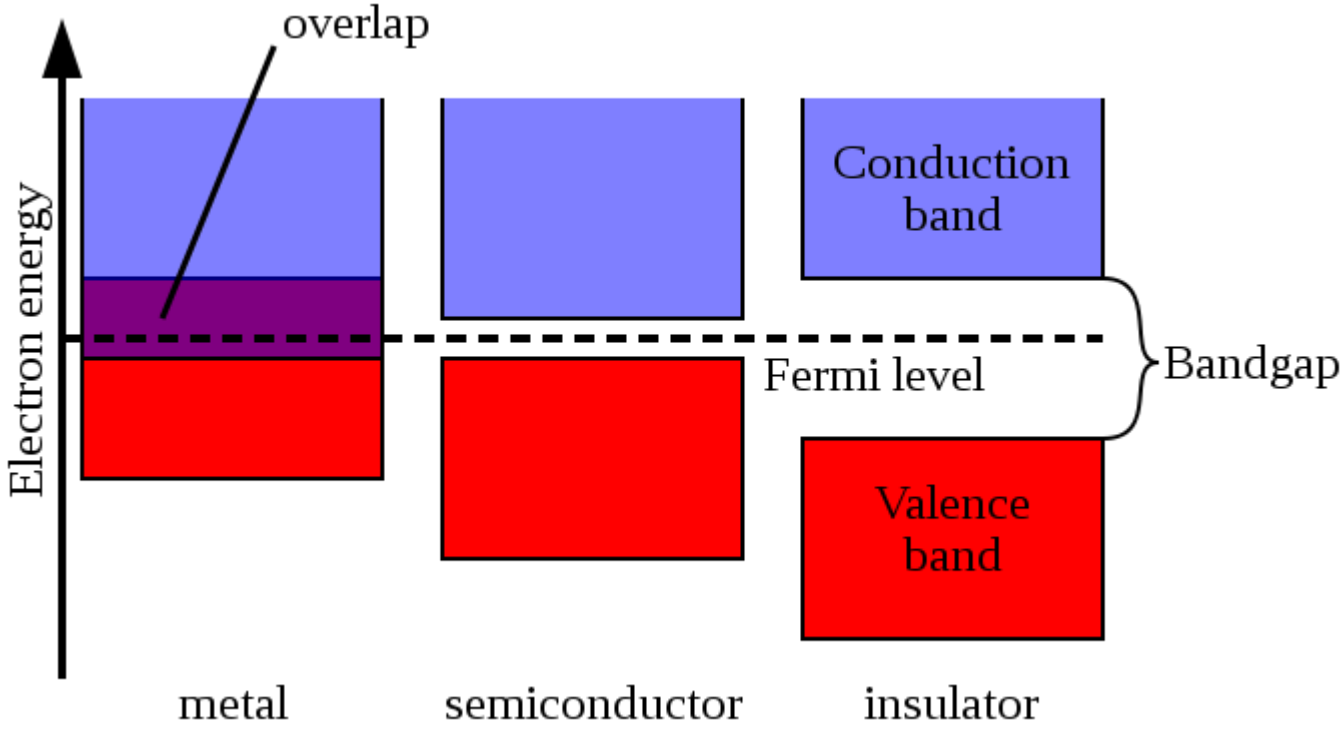
overlap
Electron energy
Conduction band
Fermi level
Bandgap
Valence band
metal
semiconductor
insulator

First Brillouin zone of FCC lattice showing symmetry labels

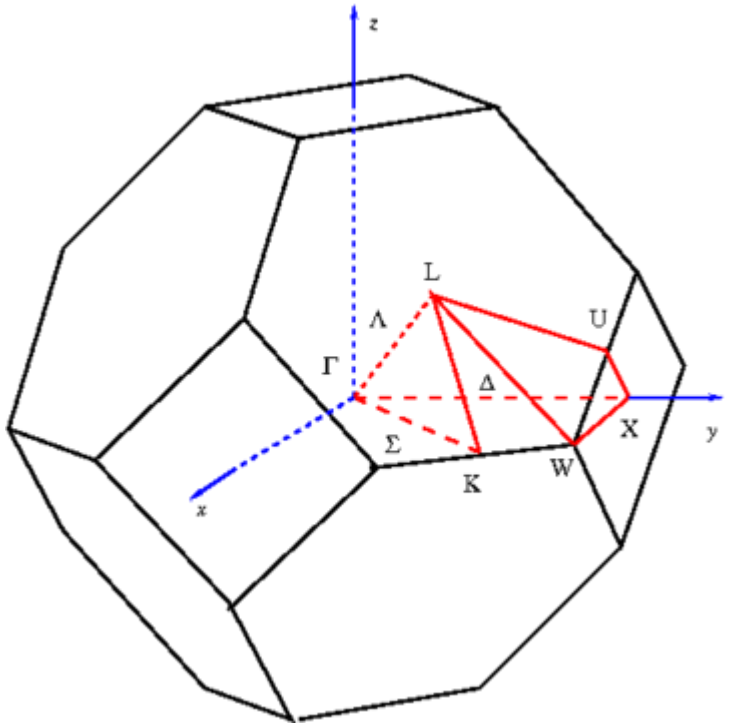

Band Structures

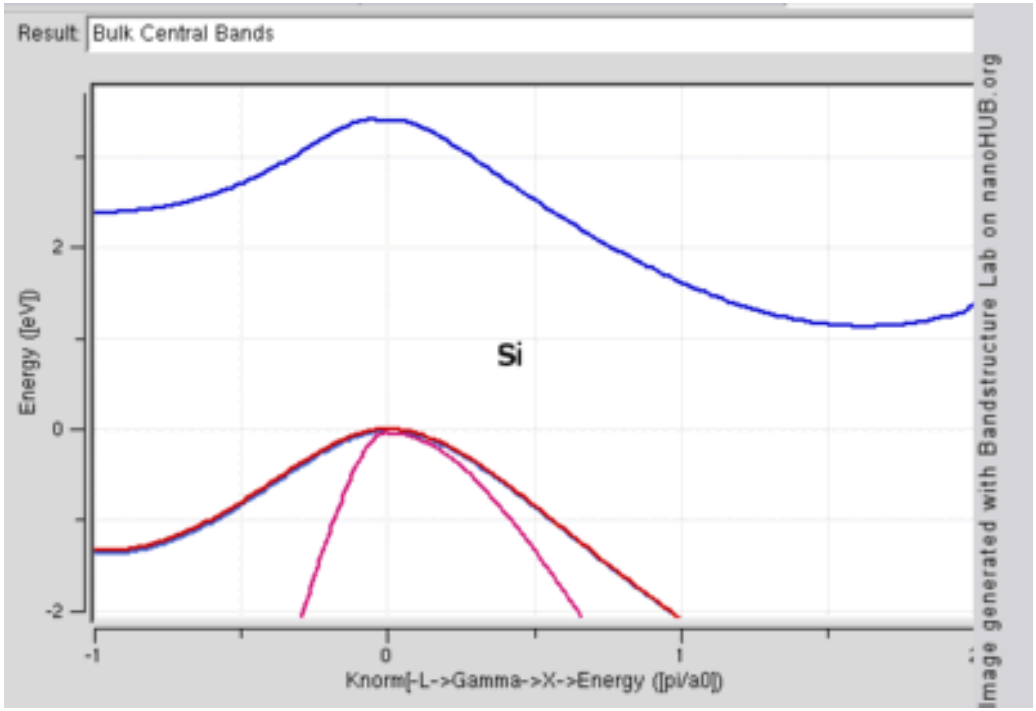

Bohr Exciton Radius

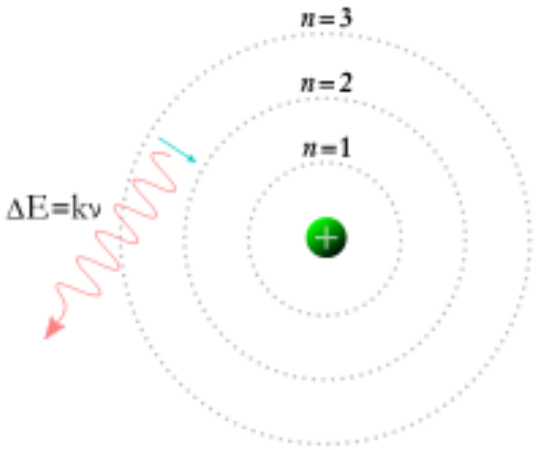

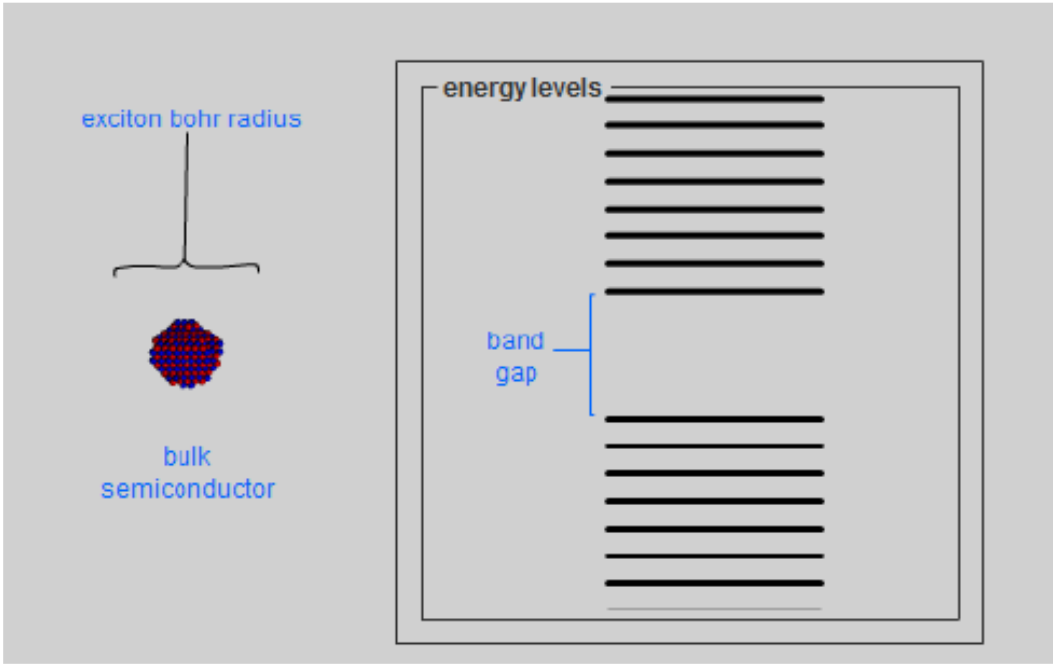

Electron Sea

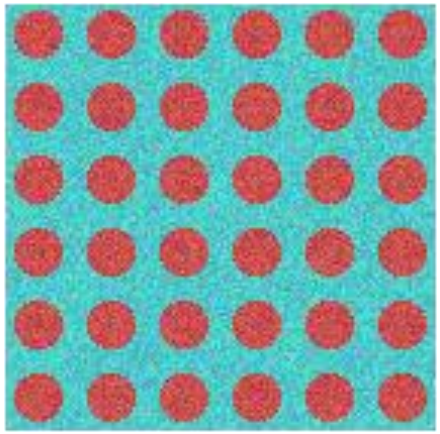

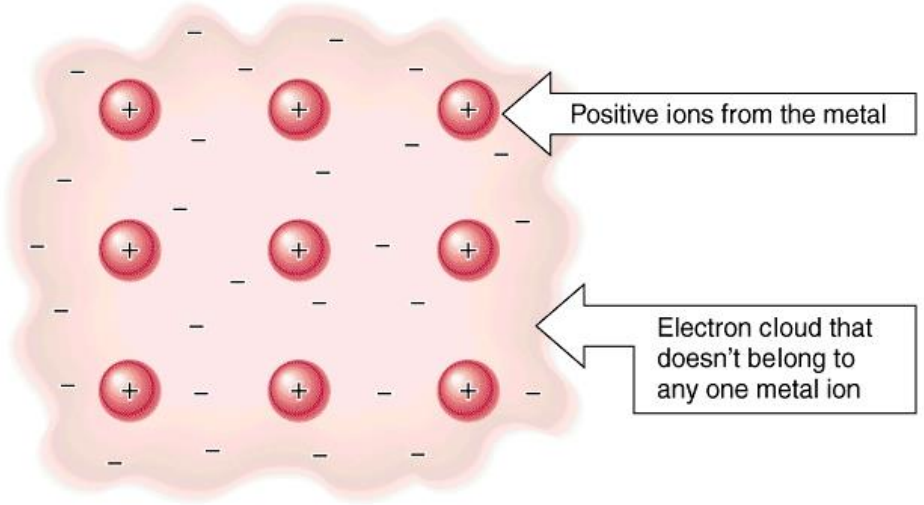

$$m\frac{d^2\delta x}{dt^2} = e\,E_x = -m\,{\omega_p}^2\,\delta x,$$

$${\omega_p}^2 = \frac{n\,e^2}{\epsilon_0\,m},$$

Surface Plasmonon

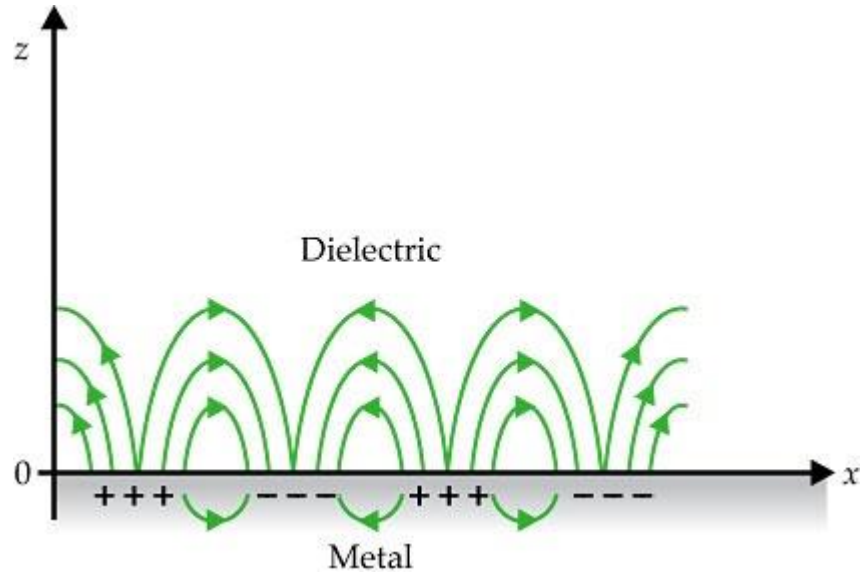

$$\varepsilon_m = 1 - \frac{\omega_p^2}{\omega^2}$$

Contact Angle

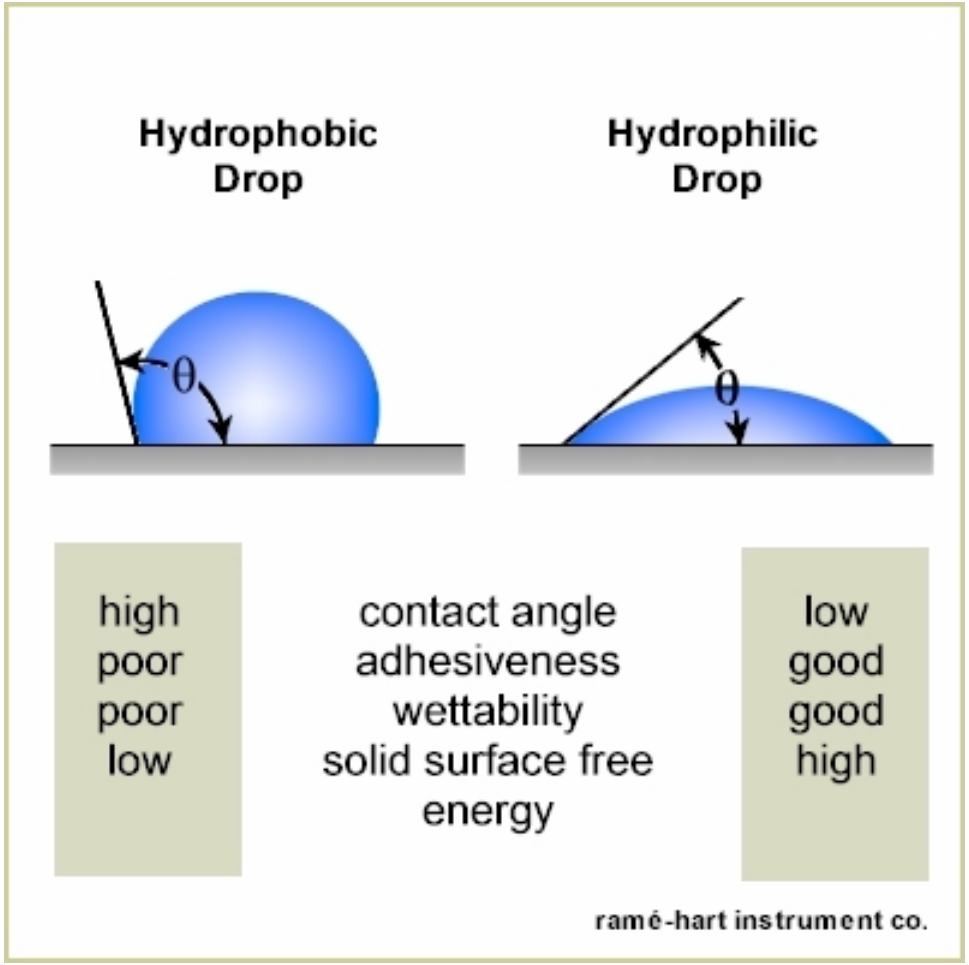

Young's Equation

$$\gamma_{SL} + \gamma_{LV} \cos\theta_c = \gamma_{SV}$$

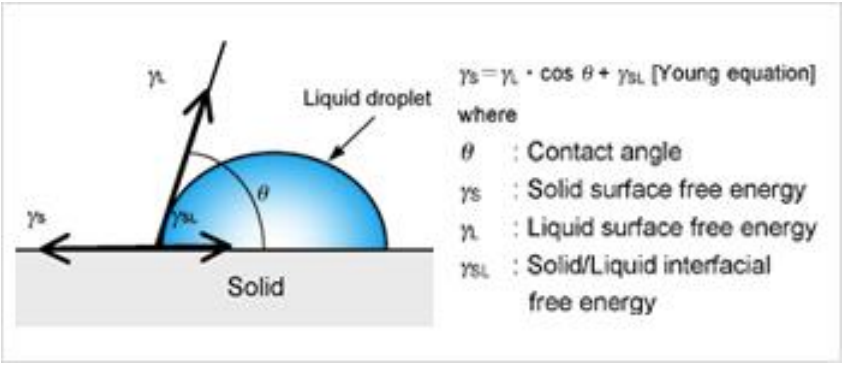

Surface Energy Minimization

- Surfactants
- DLVO
- Polymeric
- Nucleation
- Ostwald Ripening
- Sintering
- Restructure

Surfactant

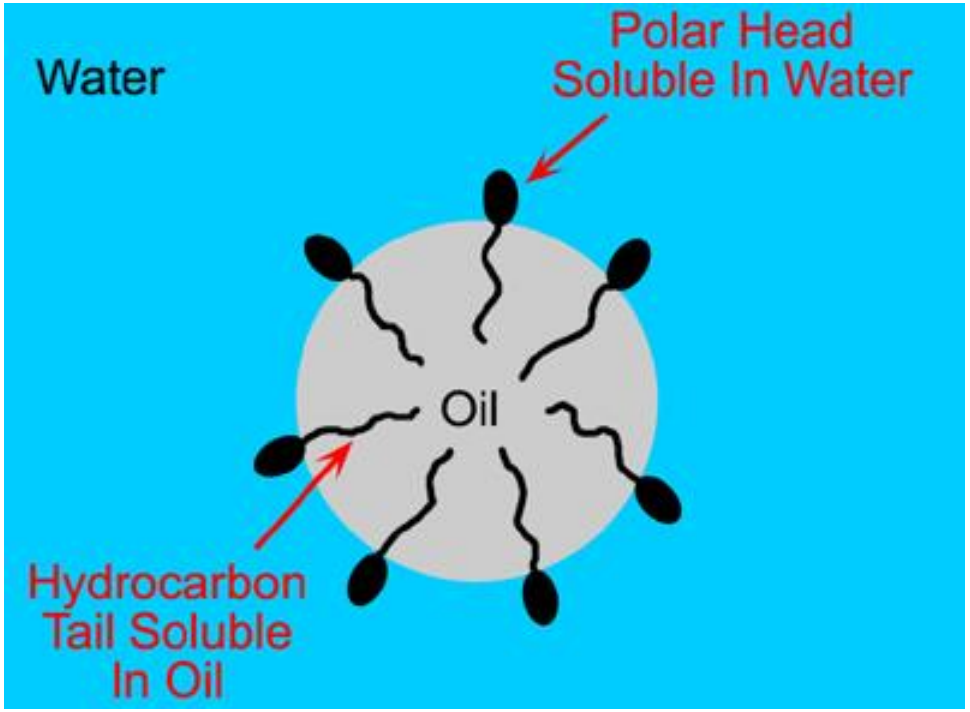
Water
Polar Head
Soluble In Water
Oil
Hydrocarbon
Tail Soluble
In Oil

DLVO Theory

$$V_T = V_A + V_R + V_S$$

$$V_A = -A/(12 \pi D^2)$$

A is the Hamaker constant and D is the particle separation

$$V_R = 2 \pi \varepsilon a \xi^2 \exp(- \kappa D)$$

a is the particle radius, π is the solvent permeability,
κ is a function of the ionic composition and ξ is the zeta potential

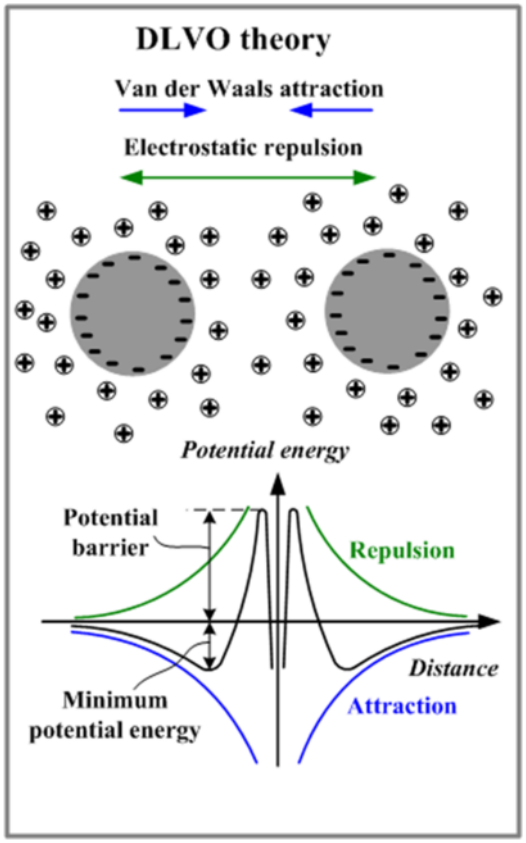

$$\omega = \omega_{el} + \omega_{vdW}$$

$$\omega = 64RTc_{\infty}{\gamma_0}^2 \frac{1}{\kappa} e^{-\kappa d} - \frac{A}{12\pi d^2}$$

$$\omega = 64RTc_{\infty}{\gamma_0}^2 \sqrt{\frac{RT\varepsilon}{F^2 \sum z^2 c_{\infty}}} e^{-\sqrt{\frac{F^2 \sum z^2 c_{\infty}}{RT\varepsilon}} d} - \frac{A}{12\pi d^2}$$

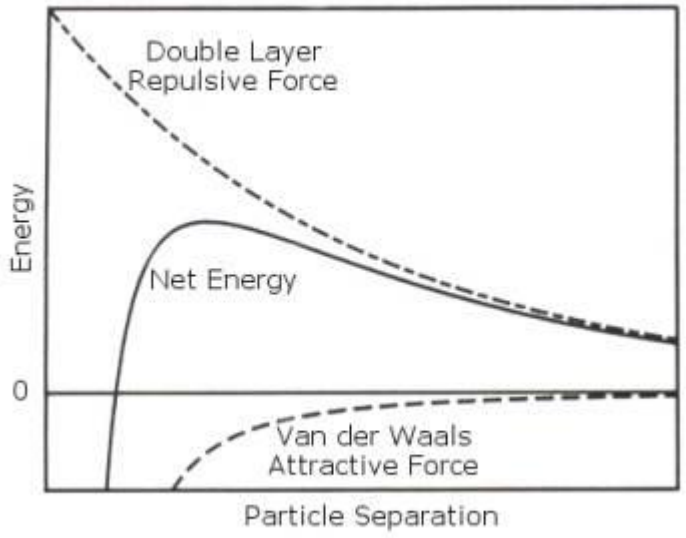
Double Layer
Repulsive Force
Energy
Net Energy
0
Van der Waals
Attractive Force
Particle Separation

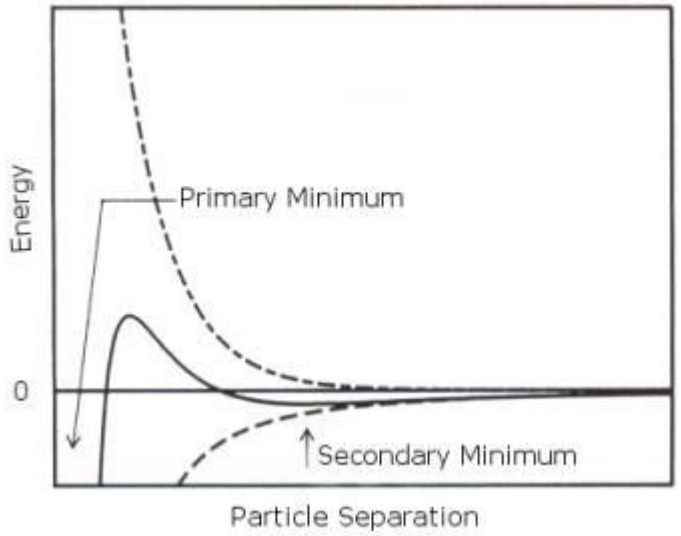
Energy
Primary Minimum
0
Secondary Minimum
Particle Separation

DLVO Theory

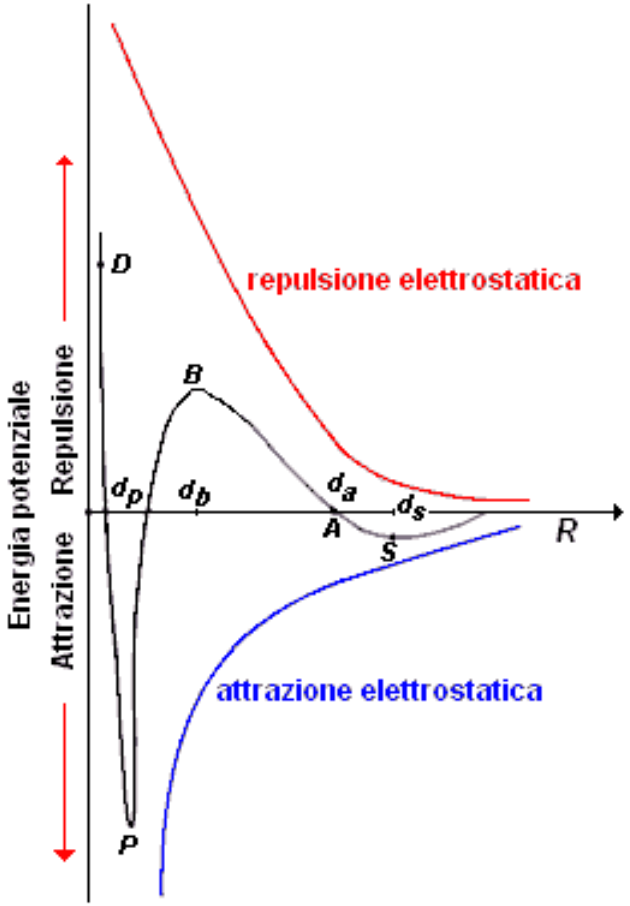
Energia potenziale
Repulsione
Attrazione
D
B
repulsione elettrostatica
d_p
d_b
d_a
d_s
A
S
R
P
attrazione elettrostatica

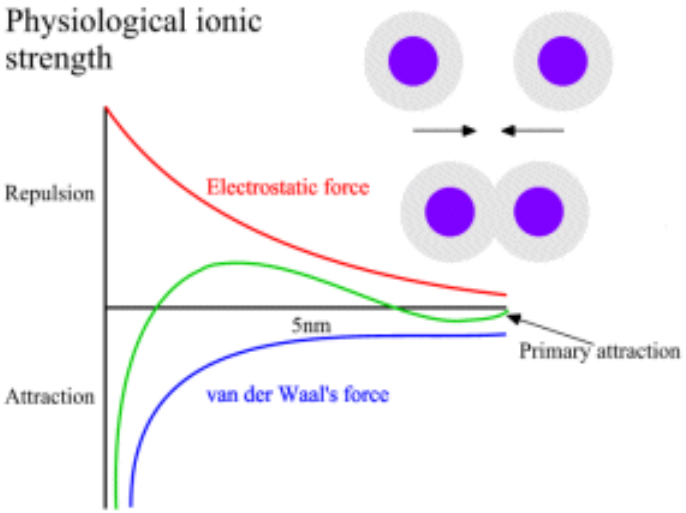
Physiological ionic strength
Repulsion
Electrostatic force
5nm
Primary attraction
Attraction
van der Waal's force

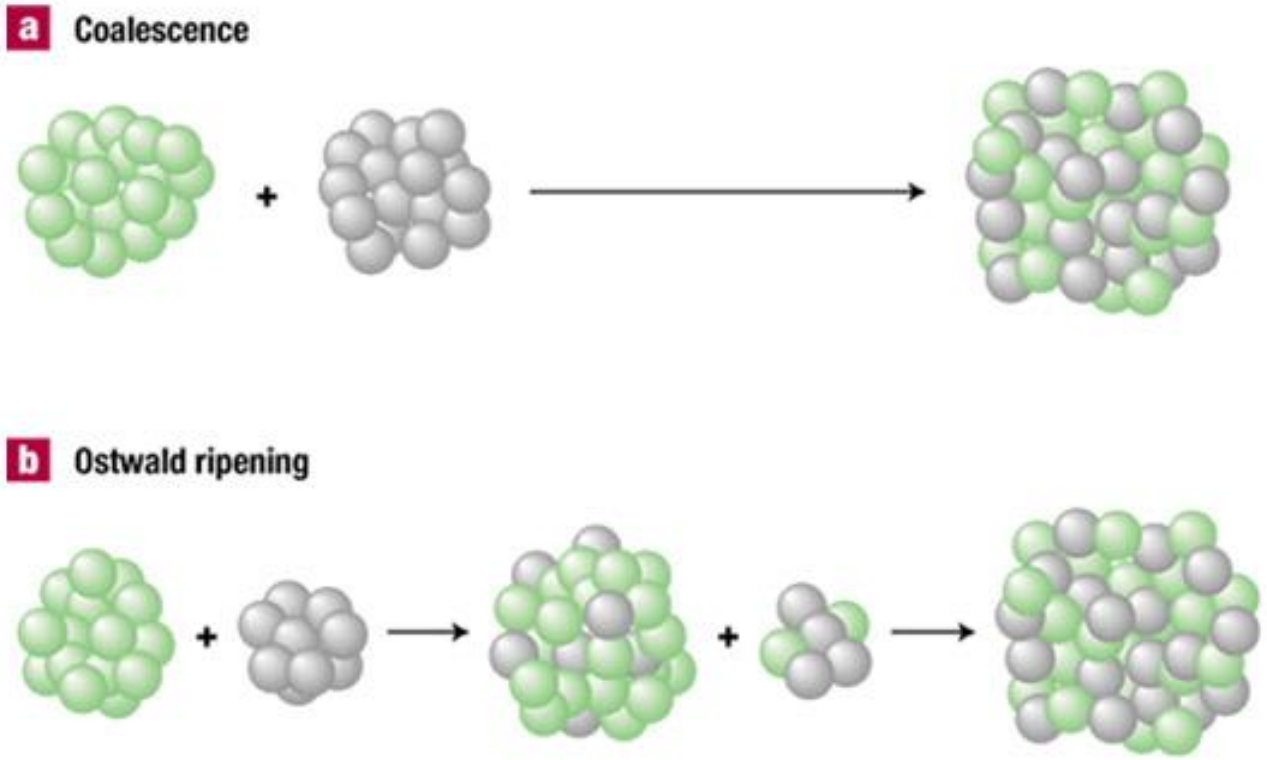

Two main mechanisms are shown here: **a**, coalescence sintering, and **b**, Ostwald ripening sintering. Coalescence sintering occurs when two clusters touch or collide and merge to form one bigger cluster. In contrast, Ostwald ripening sintering occurs by evaporation of atoms from one cluster, which then transfer to another. This is a dynamic process — both clusters exchange atoms, but the rate of loss from the smaller cluster is higher, because of the lower average coordination of atoms at the surface and their relative ease of removal. Thus big clusters get bigger at the expense of smaller clusters, which shrink and eventually disappear. The latter process is the usual form of sintering for metal clusters on a supported surface that are well spaced apart, although coalescence can occur for a high density of clusters. In general, the presence of the surface results in SMORS (surface-mediated Ostwald ripening sintering) in which material is transferred from one cluster to another by diffusion across the surface, and not through the gas phase.

Synthesis of Nanoparticles and Surface Modifications

Self-Assembly

- Static assembly
- Dynamic assembly
  - RT = 8.314 J/mol x 300 = 2.4 kJ/mol
- Driving forces
  - Chemisorption
  - Surface effect
  - Hydrophobic-hydrophilic
  - Intermolecular forces
  - Capillary force

Langmuir-Blodgett Films

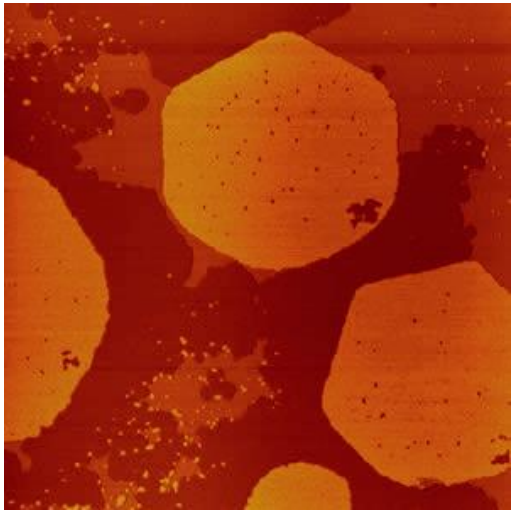

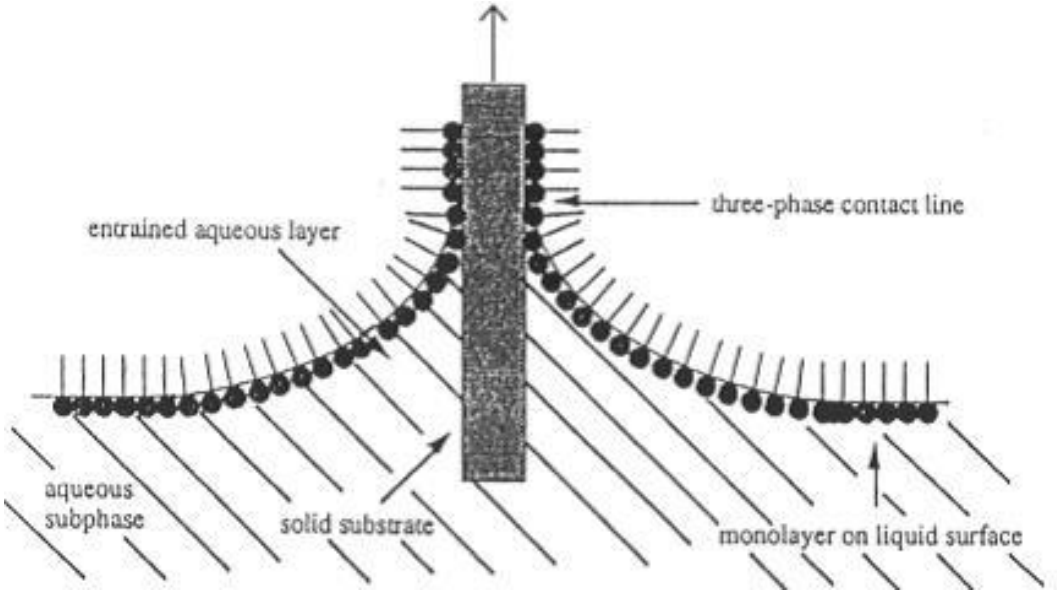

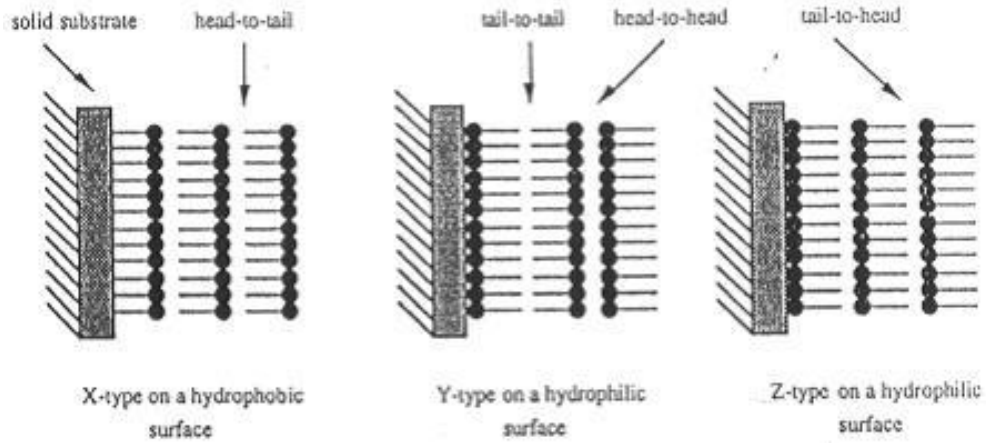

Langmuir-Blodgett Films

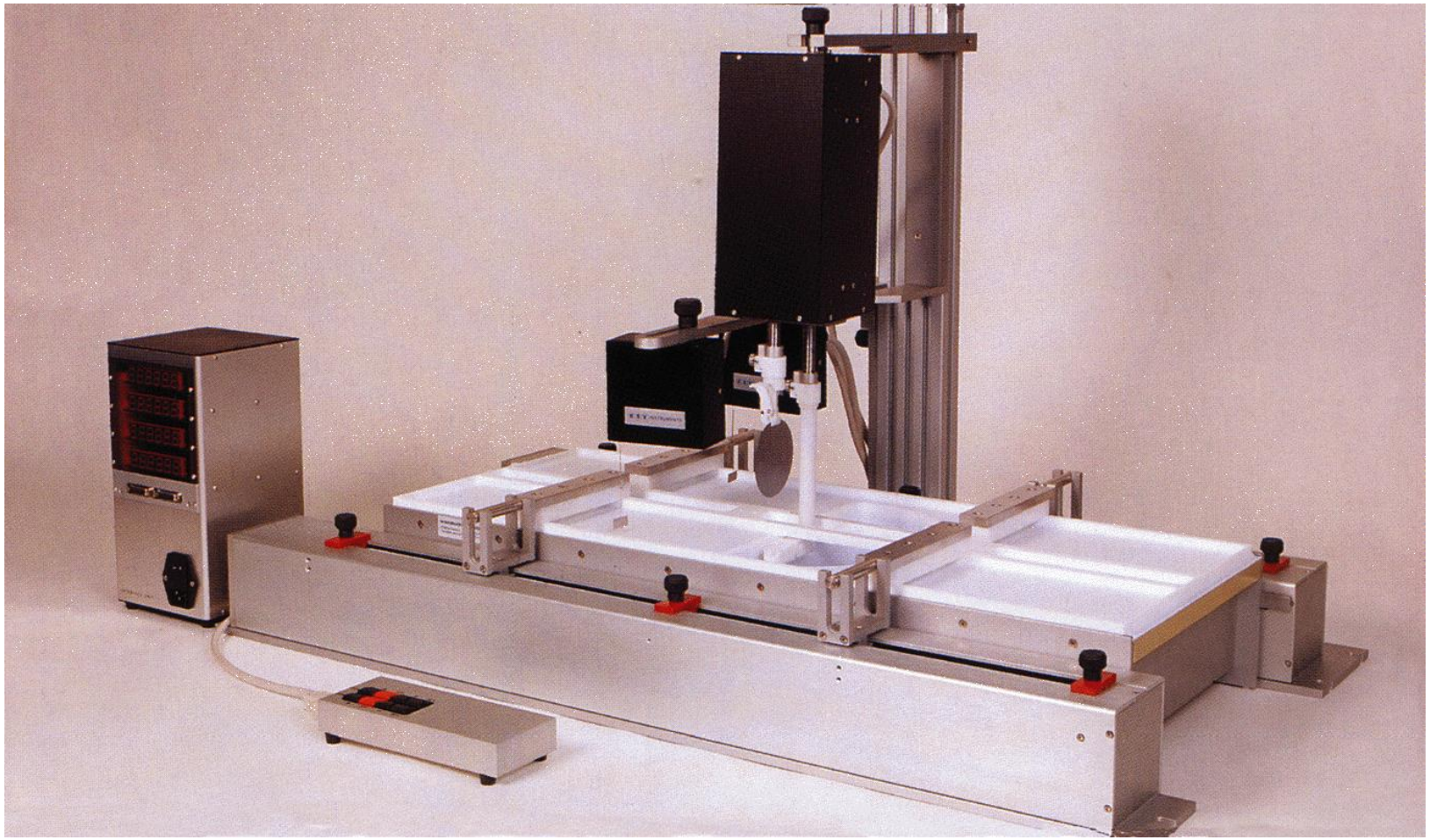

Isotherm

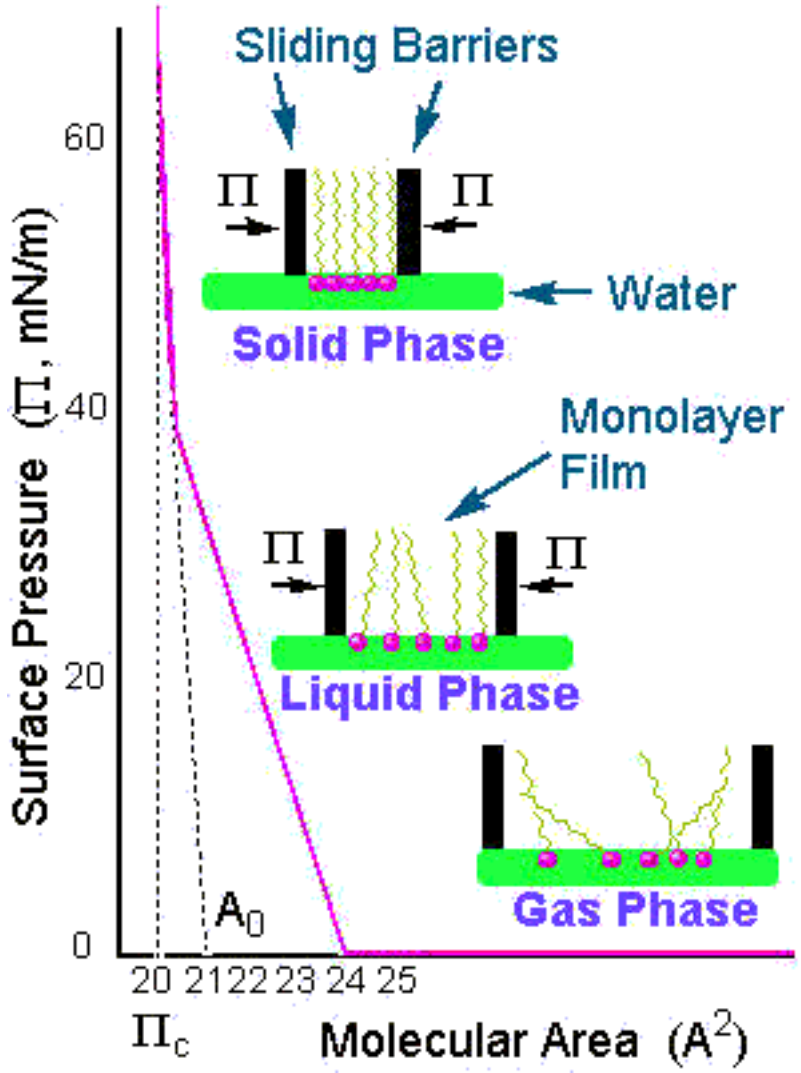
Sliding Barriers
Π
Π
Water
Solid Phase
Monolayer
Film
Liquid Phase
Gas Phase
A0
Surface Pressure (Π, mN/m)
60
40
20
0
20 21 22 23 24 25
Πc
Molecular Area (A2)

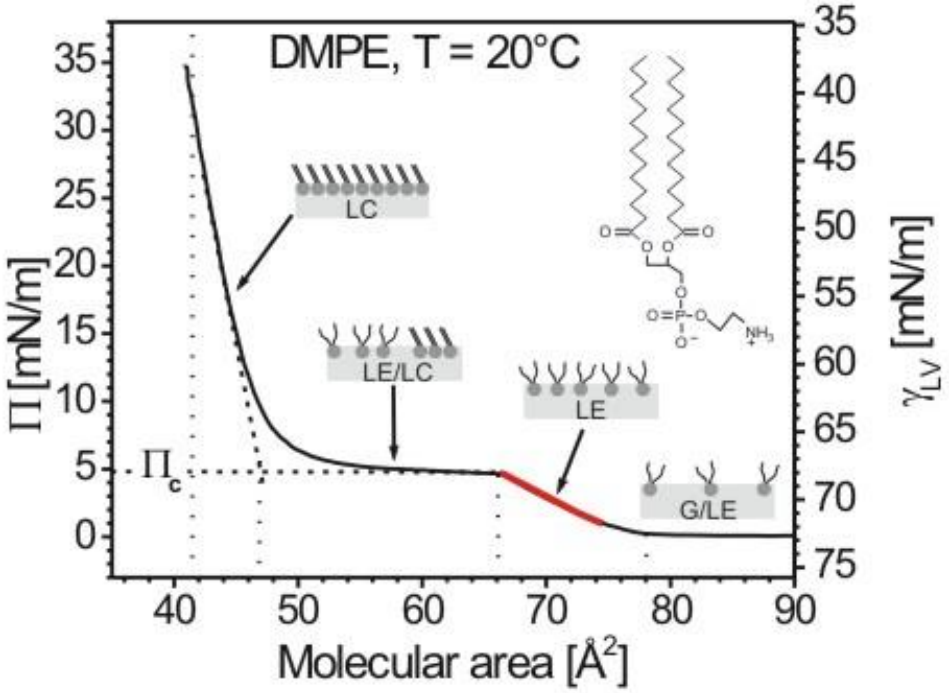
DMPE, T = 20°C
LC
LE/LC
LE
G/LE
Πc
Π [mN/m]
γLV [mN/m]
35
30
25
20
15
10
5
0
40
45
50
55
60
65
70
75
40
50
60
70
80
90
Molecular area [Å2]

Self-Assemble Monolayer (SAM)

Chem. Rev. **2005**, *105*, 1103–1169

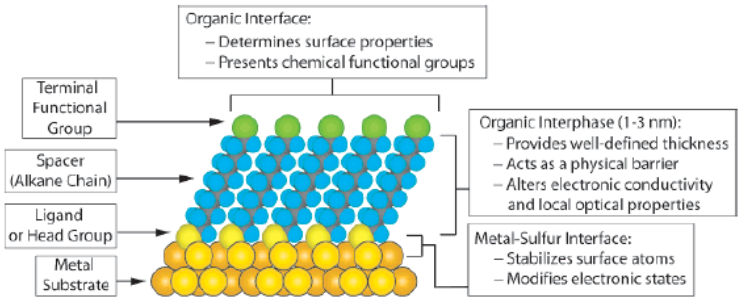

Ligand	Substrates	Morphology of Substrate: Thin Films or Bulk Material	Morphology of Substrate: Nanoparticles or Other Nanostructures
ROH	Fe_xO_y		35
	Si-H	36	
	Si	37	
RCOO-/RCOOH	α-Al_2O_3	38,39	
	Fe_xO_y		40
	Ni		41,42
	Ti/TiO_2	43	
RCOO–OOCR	Si(111):H	44	
	Si(100):H		
Ene-diol	Fe_2O_3		45
RNH_2	FeS_2	46	
	Mica	47	
	Stainless Steel 316L	48	
	$YBa_2Cu_3O_{7-\delta}$	49	
	CdSe		50
RC≡N	Ag	51	
	Au		
R-N≡N$^+$(BF_4^-)	GaAs(100)	52	
	Pd	52	
	Si(111):H	52	
RSH	Ag	26	53,54
	$Ag_{90}Ni_{10}$	55	
	AgS		56
	Au	26	57
	AuAg		58
	AuCu		58
	Au_xPd_{1-x}		58
	CdTe		59
	CdSe		60
	CdS		61,62
	Cu	26	58
	FePt		63-66
	GaAs	67	
	Ge	68	
	Hg	69-71	
	HgTe		72
	InP	73	
	Ir		74
	Ni	75	
	PbS		76-78
	Pd	30	74,79
	PdAg		58
	Pt	32	80
	Ru		81
	Stainless Steel 316L	48	
	$YBa_2Cu_3O_{7-\delta}$	82	
	Zn	83	
	ZnSe	84	
	ZnS		85
RSAc	Au	86	
	Au		87
RSR'	Au	88	

Ligand	Substrates	Morphology of Substrate: Thin Films or Bulk Material	Morphology of Substrate: Nanoparticles or Other Nanostructures
RSSR'	Ag	89	90
	Au	20	90-92
	CdS		61
	Pd	30	
	Au	93	
RCSSH	Au	94	
	CdSe		95
$RS_2O_3^-Na^+$	Au	96	98
	Cu	97	
RSeH	Ag	99	
	Au	100,101	
	CdS		60
	CdSe		102
RSeSeR'	Au	101	
R_3P	Au		103
	FeS_2	46	
	CdS		104
	CdSe		104
	CdTe		104
$R_3P=O$	Co		105,106
	CdS		104
	CdSe		104
	CdTe		104
$RPO_3^{2-}/RP(O)(OH)_2$	Al	107	
	Al-OH	108	
	$Ca_{10}(PO_4,CO_3)_6(OH)_2$	109	
	GaAs	110	
	GaN	110	
	Indium tin oxide (ITO)	111	
	Mica	112	
	TiO_2	113,114	
	ZrO_2	114,115	
	CdSe		116-118
	CdTe		118,119
RPO_4^{2-}	Al_2O_3	120	
	Nb_2O_5	120	
	Ta_2O_3	121	
	TiO_2	120,122	
RN≡C	Pt	123	124
$RHC=CH_2$	Si	37	
RC≡CH	Si(111):H	125	
$RSiX_3$ X = H, Cl, OCH_2CH_3	HfO_2	126	
	ITO	127	
	PtO	128	
	TiO_2	113,126,129	
	ZrO_2	126,129	

S-Au 25-30 Kcal/mole

Si-O 190 kcal/mole

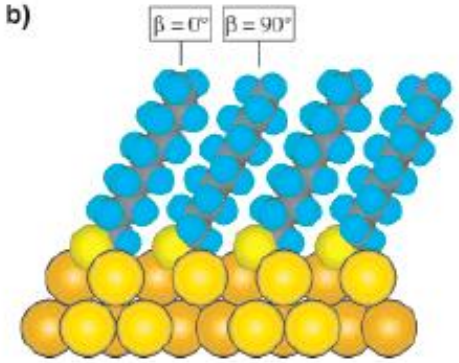

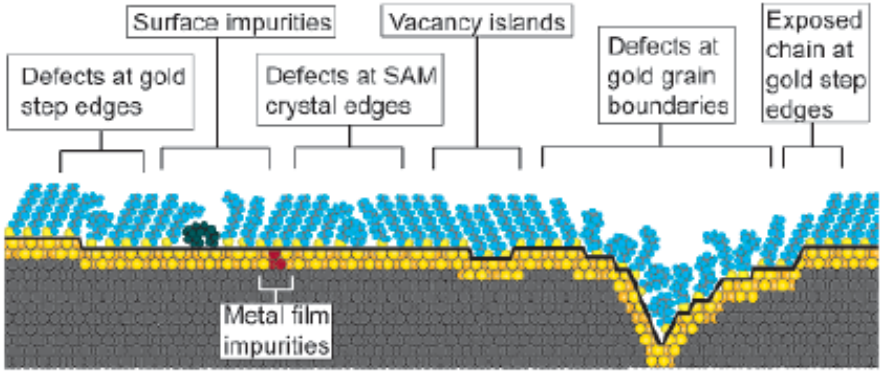

Figure 7. Schematic illustration of some of the intrinsic and extrinsic defects found in SAMs formed on polycrystalline substrates. The dark line at the metal−sulfur interface is a visual guide for the reader and indicates the changing topography of the substrate itself.

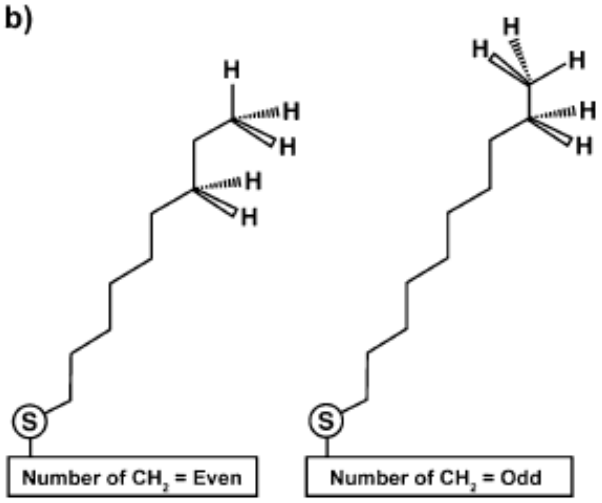

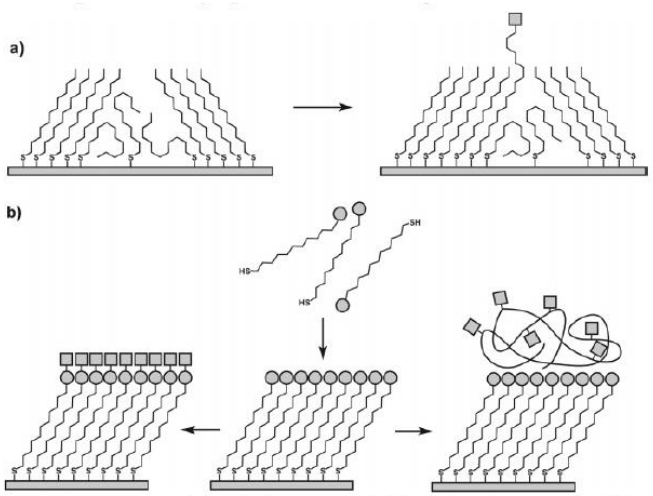

[c] (a) Insertion of a functional adsorbate at a defect site in a preformed SAM. (b) Transformation of a SAM with exposed functional groups (circles) by either chemical reaction or adsorption of another material.

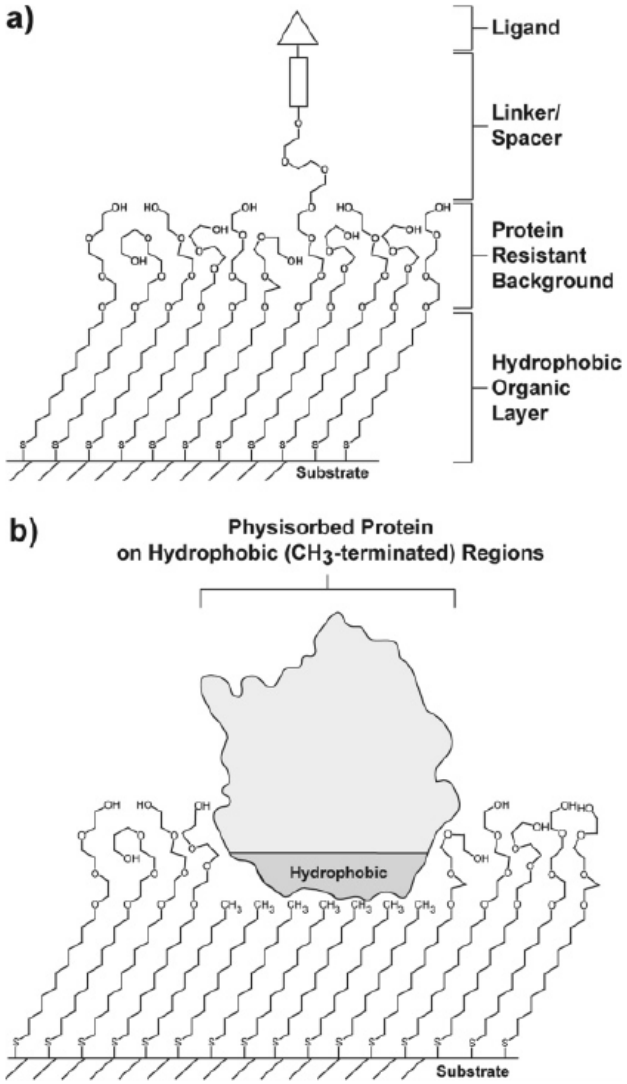

Figure 21. Schematic illustrations of (a) a mixed SAM and (b) a patterned SAM. Both types are used for applications in biology and biochemistry.

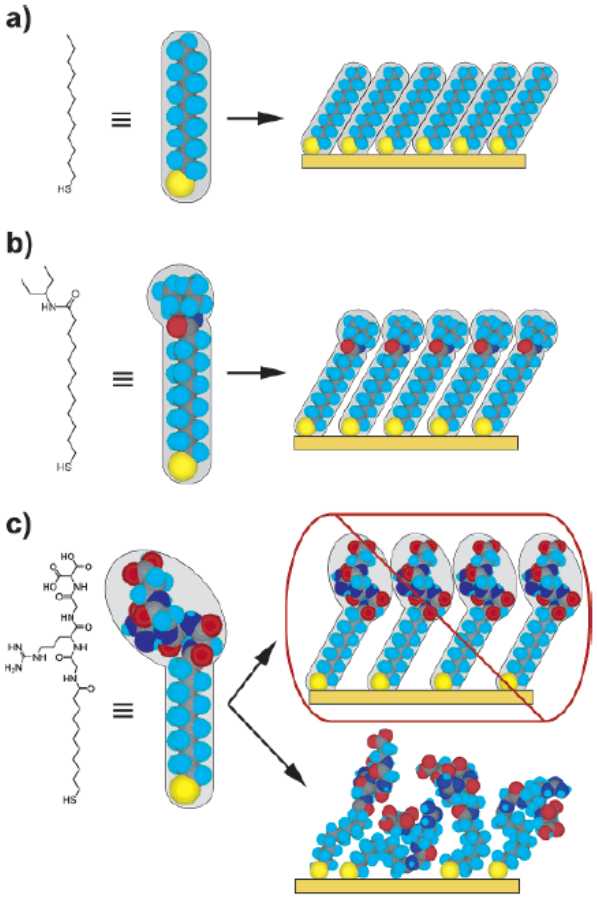

Figure 22. Schematic diagram illustrating the effects that large terminal groups have on the packing density and organization of SAMs. (a) Small terminal groups such as $-CH_3$, $-CN$, etc., do not distort the secondary organization of the organic layer and have no effect on the sulfur arrangement. (b) Slightly larger groups (like the branched amide shown here) begin to distort the organization of the organic layer, but the strongly favorable energetics of metal−sulfur binding drive a highly dense arrangement of adsorbates. (c) Large terminal groups (peptides, proteins, antibodies) sterically are unable to adopt a secondary organization similar to that for alkanethiols with small terminal groups. The resulting structures probably are more disordered and less dense than those formed with the types of molecules in a and b.

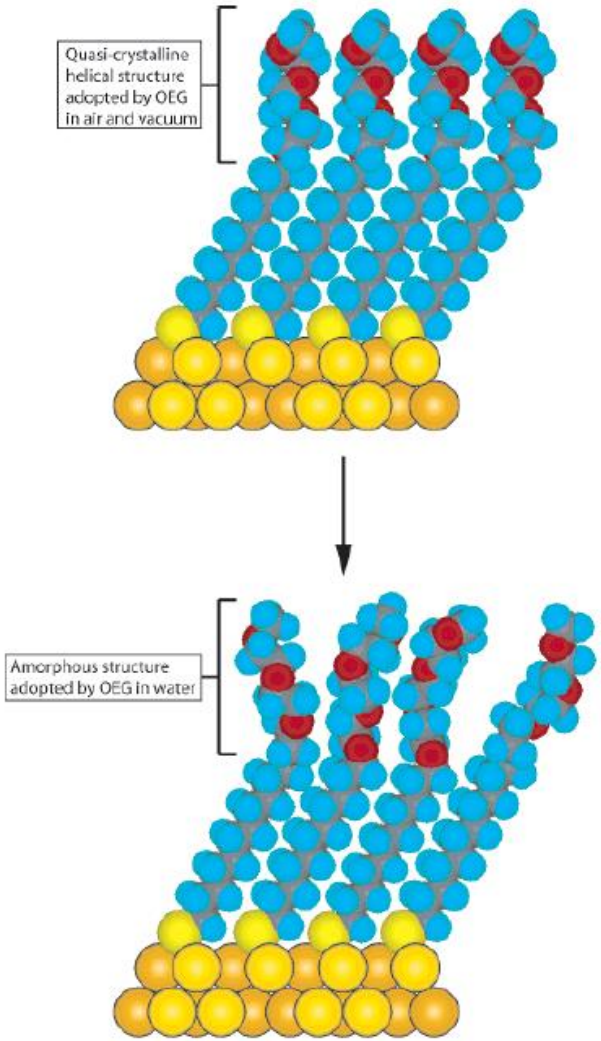

Figure 23. Schematic illustration of the order−disorder transition evidenced by SAMs of alkanethiolates terminated with triethylene glycol. The EG_3 group loses conformational ordering upon solvation in water.

Temperature Programmed Desorption

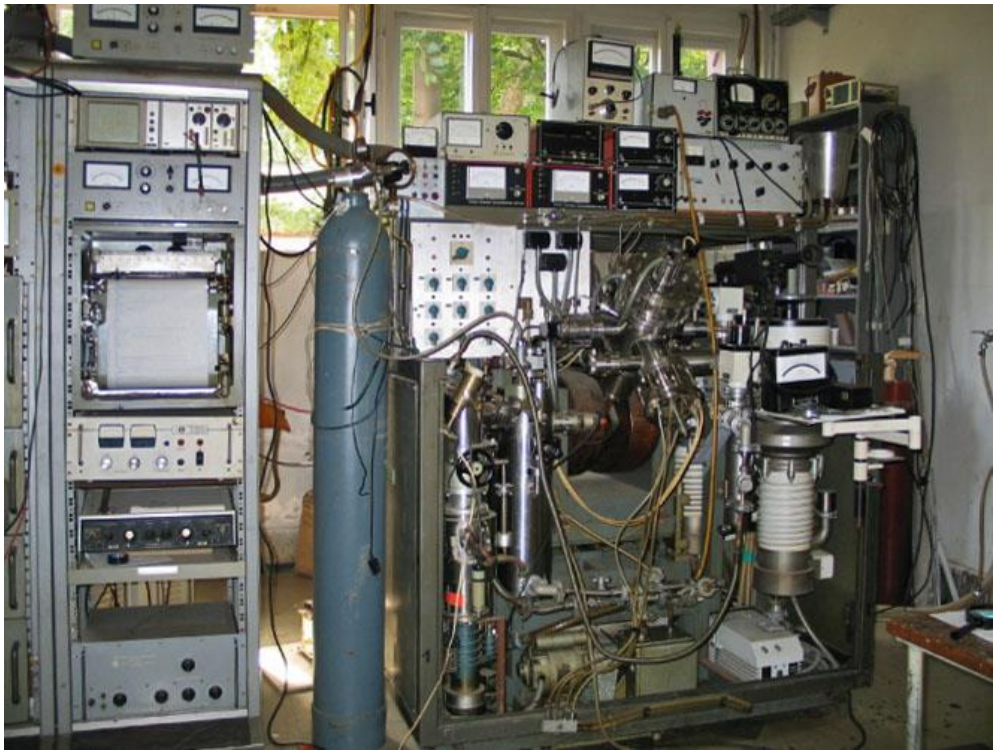

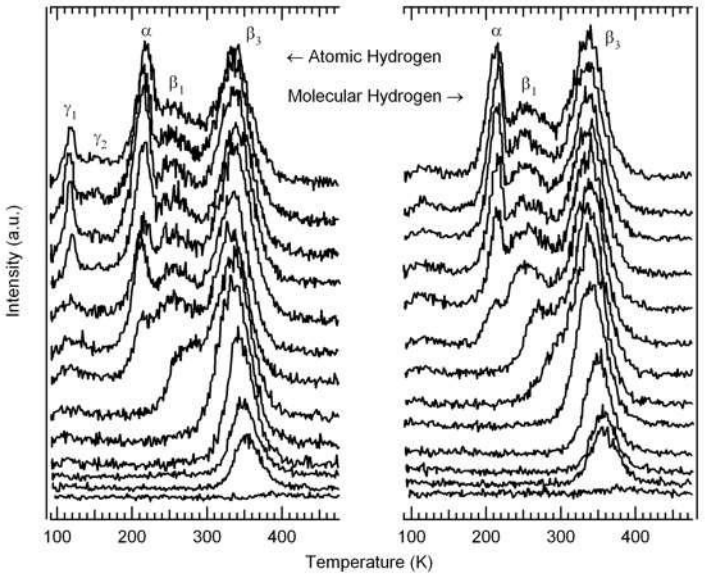

Self-Assembly

- Substrates
- Interstitial adhesion layer
- Noble metal layer
- Organo-sulfur

Synthesis of Silver Nanoparticles

1. *A solution of $AgNO_3$ (1.0×10^{-3} M) in deionized water was heated until it began to boil.*
2. *Sodium citrate solution was added dropwise to the silver nitrate solution as soon as the boiling commenced. The color of the solution slowly turned into grayish yellow, indicating the reduction of the Ag+ ions.*
3. *Heating was continued for an additional 15 min, and then the solution was cooled to room temperature before employing for further experimentation.*

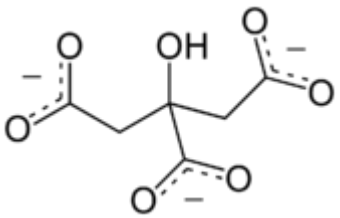

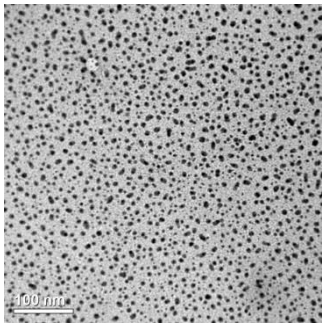

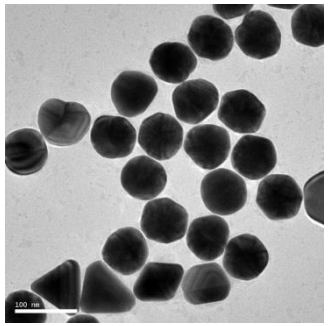

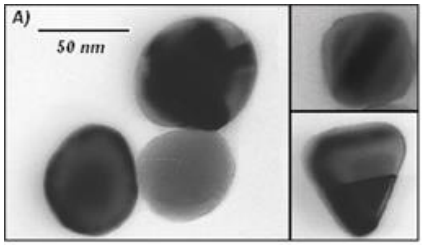

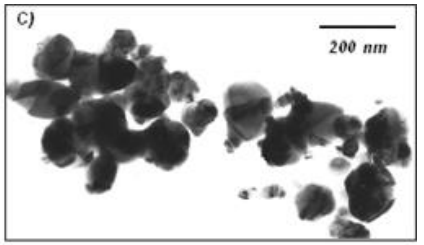

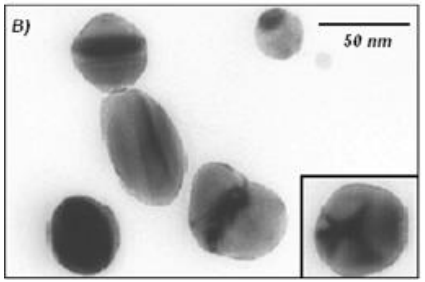

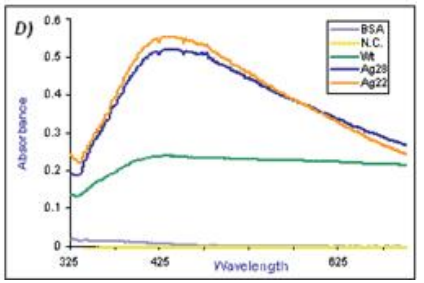

Synthesis of Gold Nanoparticles

1. *Add 20 mL of 1.0 mM $HAuCl_4$ to a 50 mL round bottom flask on a stirring hot plate.*
2. *Add a magnetic stir bar and bring the solution to a boil.*
3. *To the boiling solution, add 2 mL of a 1% solution of trisodium citrate dihydrate*
4. *The gold sol gradually forms as the citrate reduces the gold(III). Stop heating when a deep red color is obtained.*

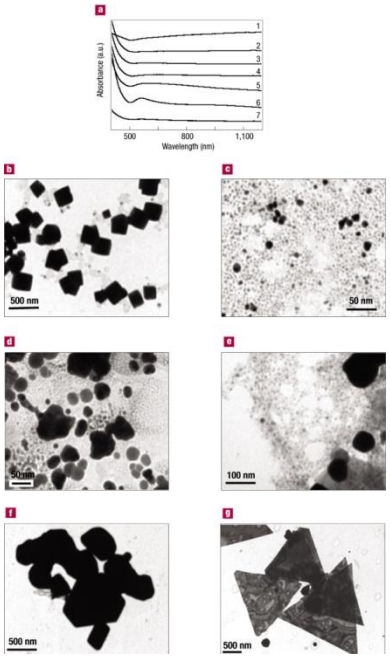

$$(1)\quad M_xO_y \xrightarrow[(\text{medium})\ \Delta_T]{\text{Reducing Agent}} M_n + H_2O$$

(Reducing Agent = R - COH)

$$(2)\quad M(L)_x \xrightarrow[(\text{medium})\ \Delta_T]{\text{Reducing Agent}} M_n + L^-$$

$(L = NO_3^-, C_2H_5O^-)$

(Reducing Agent = R - COH)

Construction of Core Shell Ag/Au@SiO_2 Nanoparticles

1. *Under vigorous stirring, 1 ml of the silver/ gold colloids solution was mixed with 250 mL of isopropanol and 25 mL of deionized water.*
2. *Immediately after the addition of 4 mL of 30% ammonium hydroxide, different amounts of tetraethoxysilane (TEOS) were added to the reaction mixture.*
3. *To obtain different silica layer thicknesses, TEOS solutions with a concentration between 50% and 100% was added to the suspension. The reaction was stirred at room temperature for 30 minutes and then was allowed to age without agitation at 4 ℃ overnight.*
4. *Each suspension of silica-coated silver/gold nanoparticles was washed and centrifuged, followed by re-suspension in water. The thickness of the silica layers was determined from TEM images .*

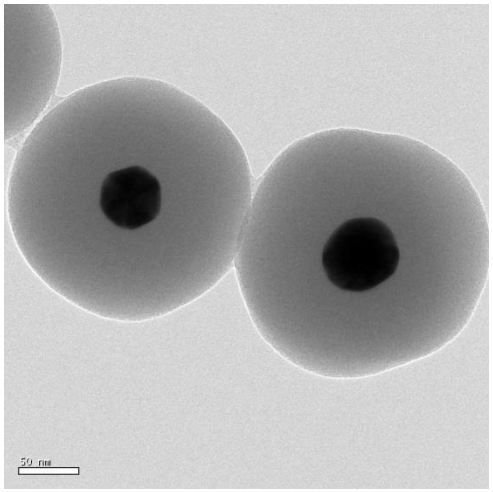

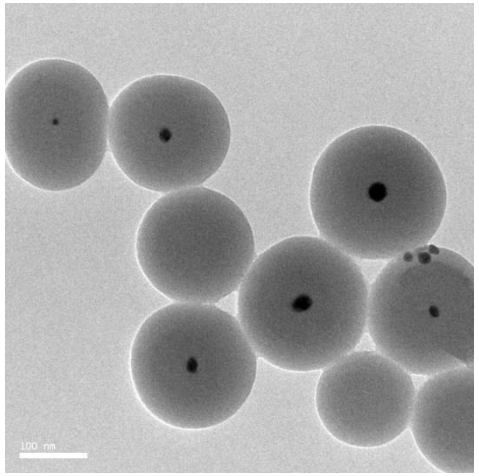

Core-Shell Nanoparticles

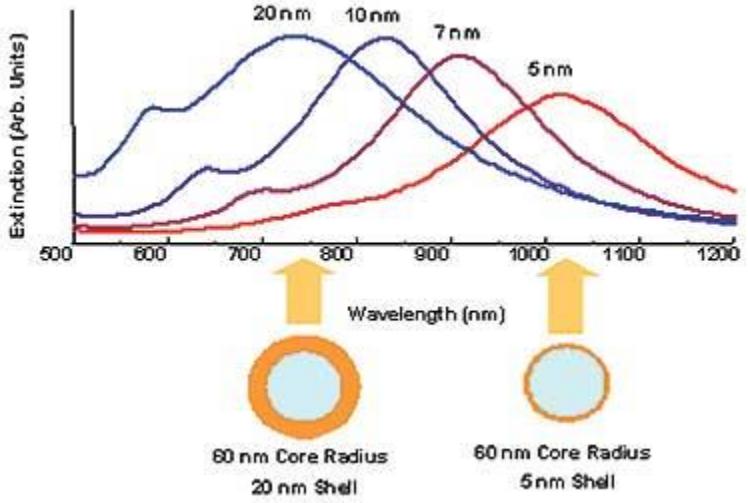

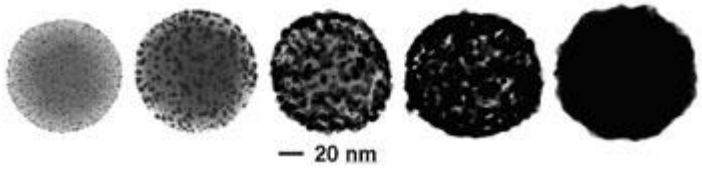

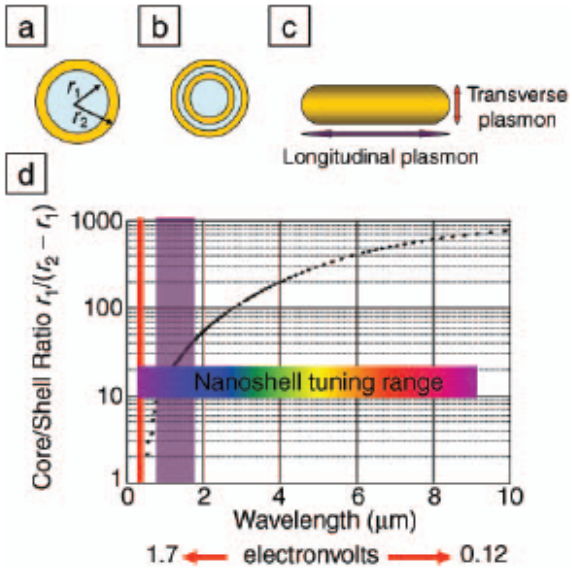

Figure 1. (a) Schematic illustration of a silica-core, gold-shell nanoshell, indicating inner (r_1) and outer (r_2) radii of the shell layers. (b) Depiction of a four-layer, concentric nanoshell. (c) Schematic illustration of a metallic nanorod. (d) Plot of nanoshell resonance as a function of core and shell dimensions, overlaid with reported spectral ranges of nanorod resonances (red, transverse plasmon; purple, longitudinal plasmon), and reported nanoshell and concentric nanoshell combined spectral range of plasmon response.

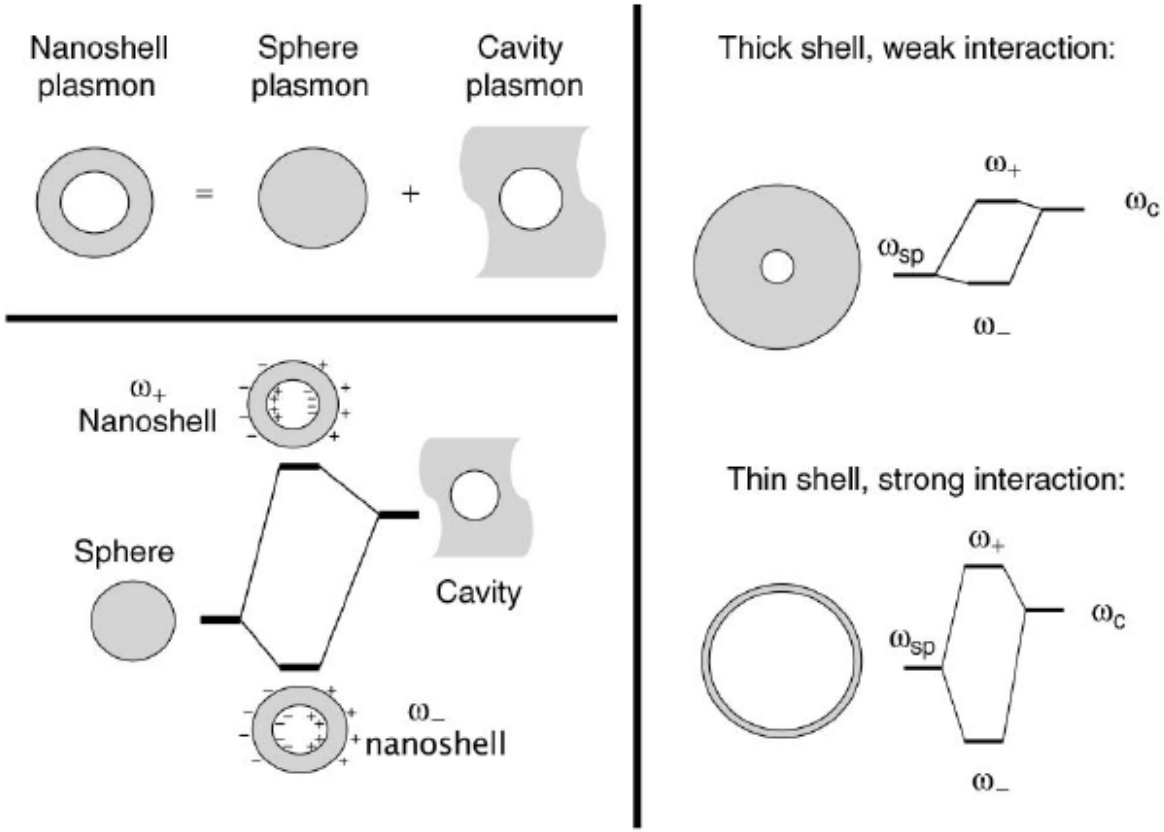

Figure 2. Plasmon hybridization and the sphere–cavity model for nanoshells: the interaction between a sphere (resonance frequency, ω_{sp}) and a cavity plasmon (resonance frequency, ω_c) is tuned by varying the thickness of the shell layer of the nanoparticle. Two hybrid plasmon resonances, the ω_- "bright," or "bonding," plasmon and the ω_+ "dark," or "anti-bonding," plasmon resonances are formed. The lower-energy plasmon couples most strongly to the optical field.

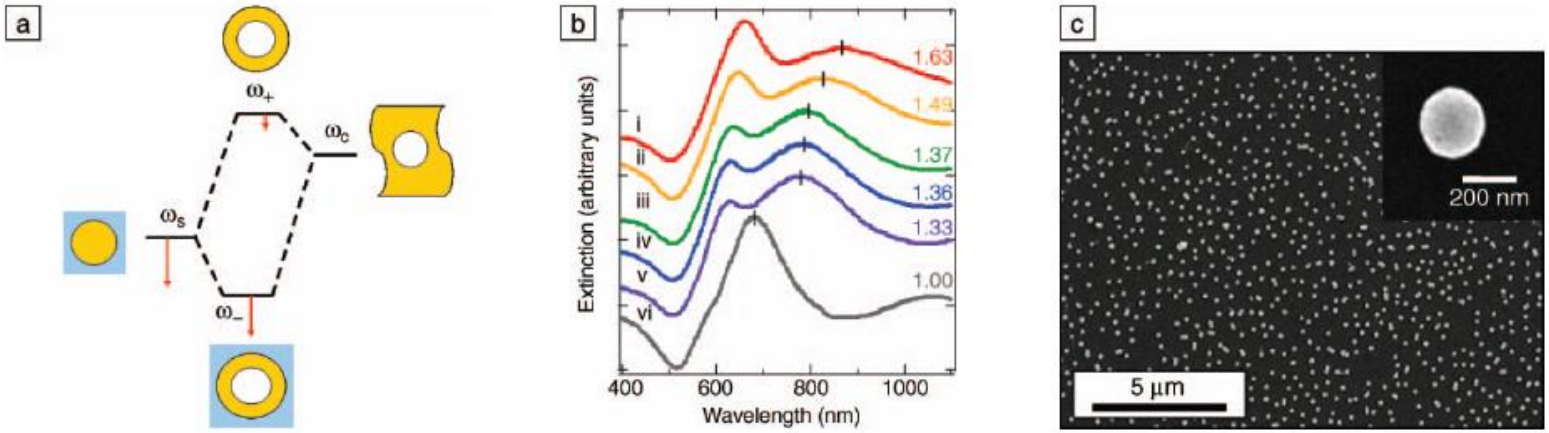

Figure 5. (a) Plasmon hybridization picture applied to surface plasmon resonance sensing with nanoshells: the low-energy "bonding" plasmon, ω_- , is sensitized to changes in its dielectric environment. The blue background schematically denotes the embedding medium for the nanoparticle. (b) Experimental curves showing plasmon resonance shifts for nanoshell-coated films in various media: (i) carbon disulfide, (ii) toluene, (iii) hexane, (iv) ethanol, (v) H_2O, and (vi) air. The index of refraction for each embedding medium is noted on the far right of the spectra. Spectra are offset for clarity. (c) Scanning electron micrograph of nanoshells deposited onto a poly(vinyl pyridine) functionalized glass surface, as used to acquire data in (b). Inset: individual nanoshell.

Preparation of Fe_3O_4@Ag/Au

1. *To the magnetic nanoparticle suspension obtained from commercial company, add 50 ml of a solution of Au (III) salt or Ag (I) salt at concentration of 0.01–1% mmol/L , shaking for 30 minutes, allowing Au (III) or Ag (I) ion to absorb on the surface of magnetic nanoparticle sufficiently,*
2. *Then adding 15–40 ml of reducing agent, such as hydroxylamine hydrochloride at concentration of 40 mmol/L, reacting for 5–40 minutes.*
3. *Further adding 1–10 ml of a solution of Au (III) salt or Ag (I) salt at concentration of 0.01–1%, shaking for 10 minutes, coating a reduced layer of gold or silver on the surface of the magnetic nanoparticle, forming super-paramagnetic composite particles having core/shell structure, separating magnetically, washing repeatedly with distilled water.*

.

Synthesis of Quantum Dots

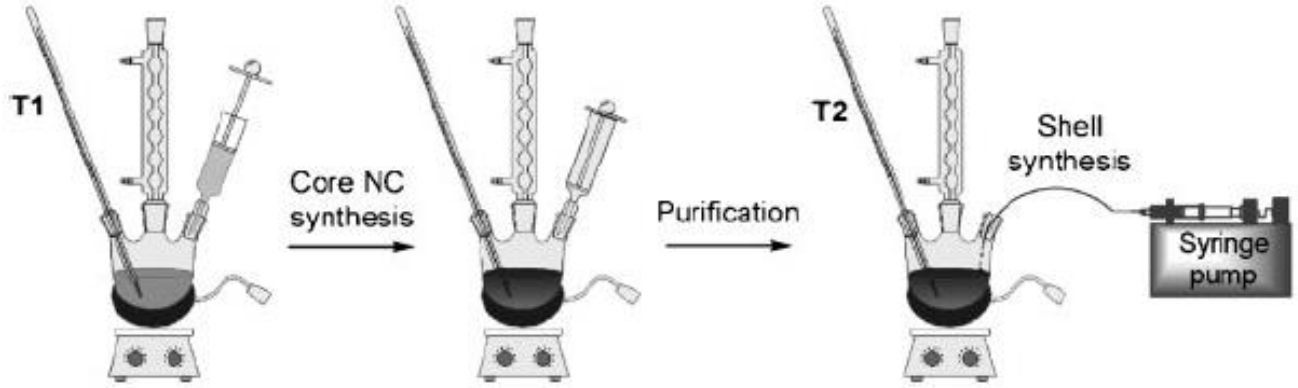

Figure 2. Two–step synthesis of core/shell nanocrystals.

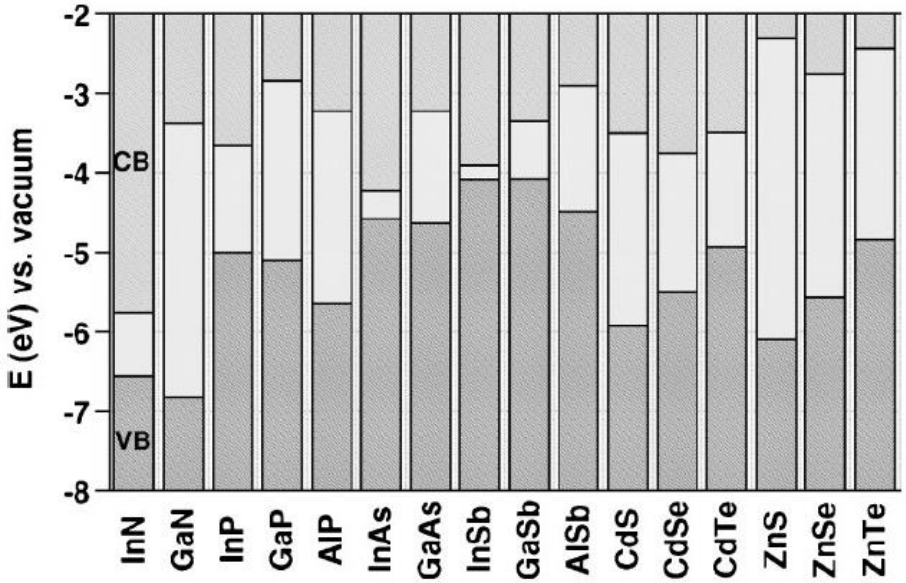

Scheme 1. Electronic energy levels of selected III–V and II–VI semiconductors using the valence-band offsets from Reference [12] (VB: valence band, CB: conduction band).

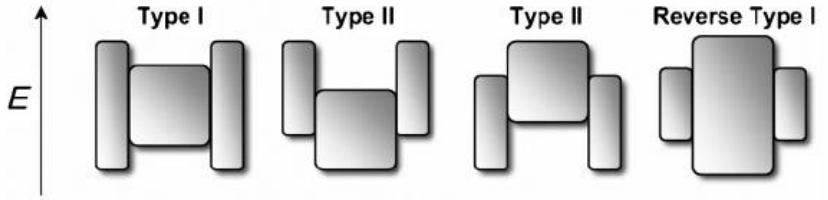

Figure 1. Schematic representation of the energy-level alignment in different core/shell systems realized with semiconductor NCs to date. The upper and lower edges of the rectangles correspond to the positions of the conduction- and valence-band edge of the core (center) and shell materials, respectively.

Template Synthesis

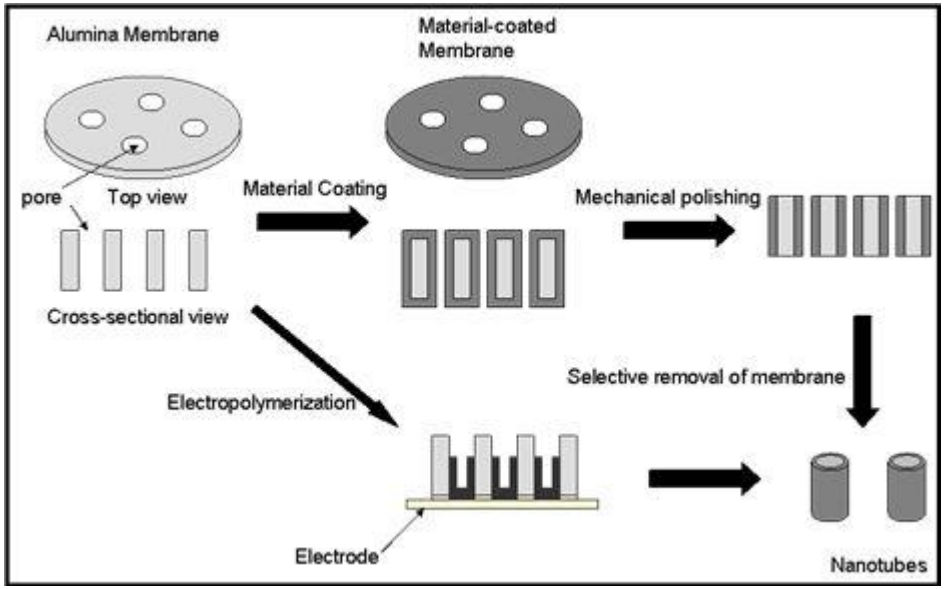

Porous Materials

- AAO
- MCM-41

Mobil Crystalline Materials, or MCM-41

Santa Barbara Amorphous type material, or SBA-15

- Micro: < 2nm
- Meso:
- Macro: > 50nm

AAO

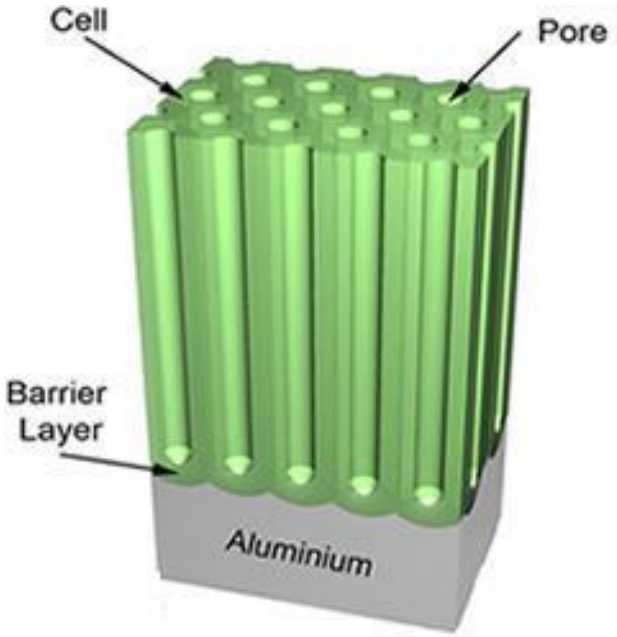

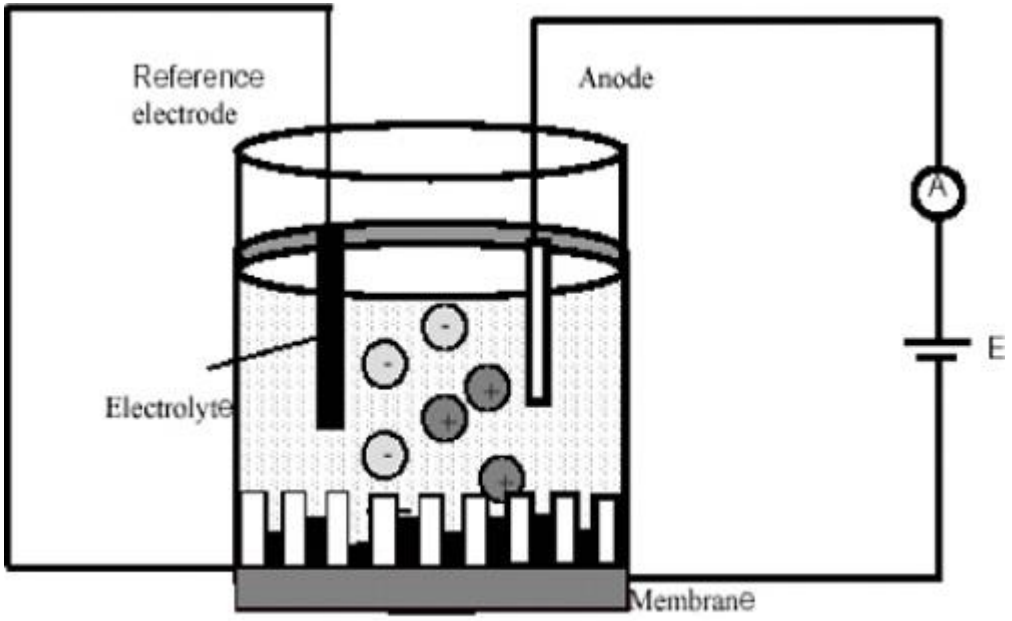

Cathode; sputter deposited Au

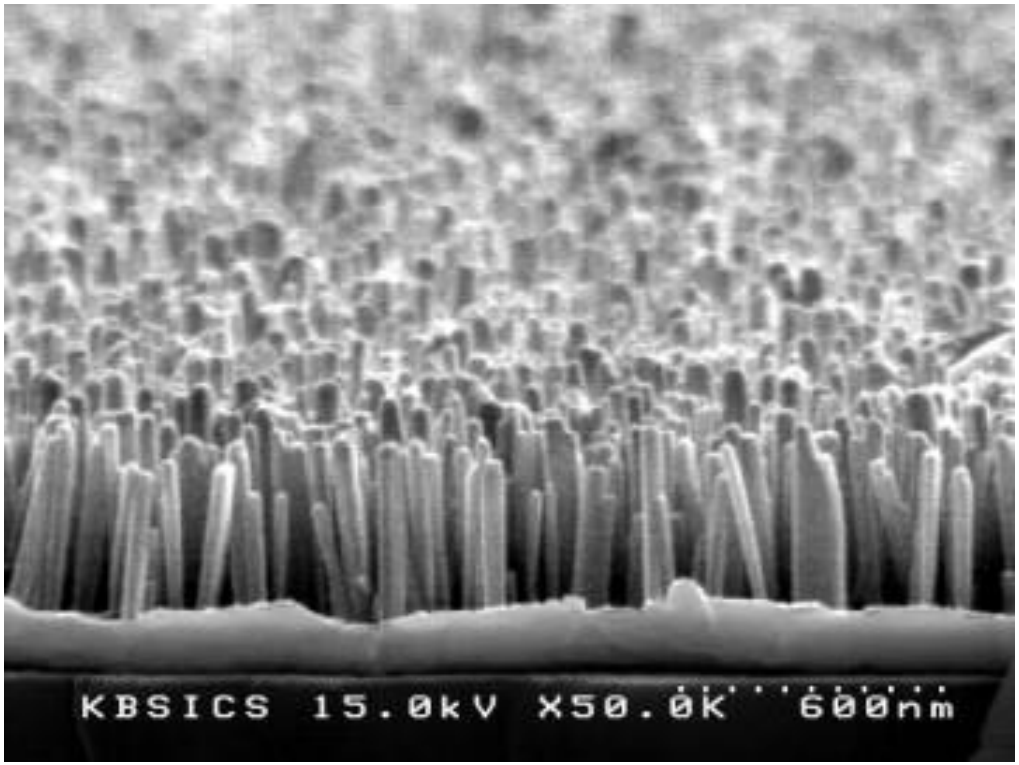
KBSICS 15.0kV X50.0K 600nm

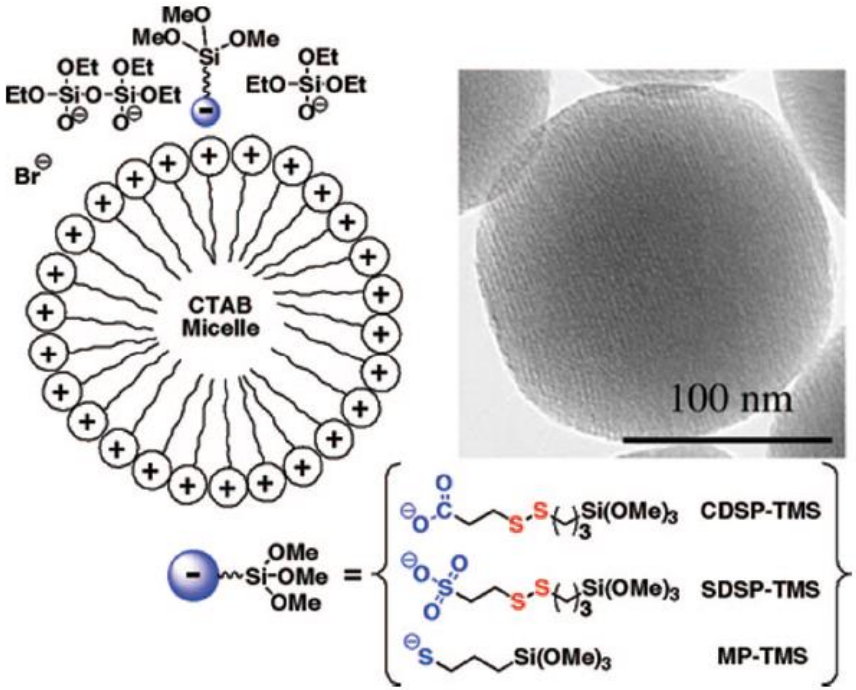

FIGURE 3. Schematic representation of the use of anionic organoalkoxysilanes for controlling the functionalization of the MSN materials. The MCM-41-type mesoporous channels are illustrated by the parallel stripes shown in the transmission electron microscopy (TEM) micrograph of the MSN–SH material. Reproduced with permission from ref 15. Copyright 2005, Royal Society of Chemistry.

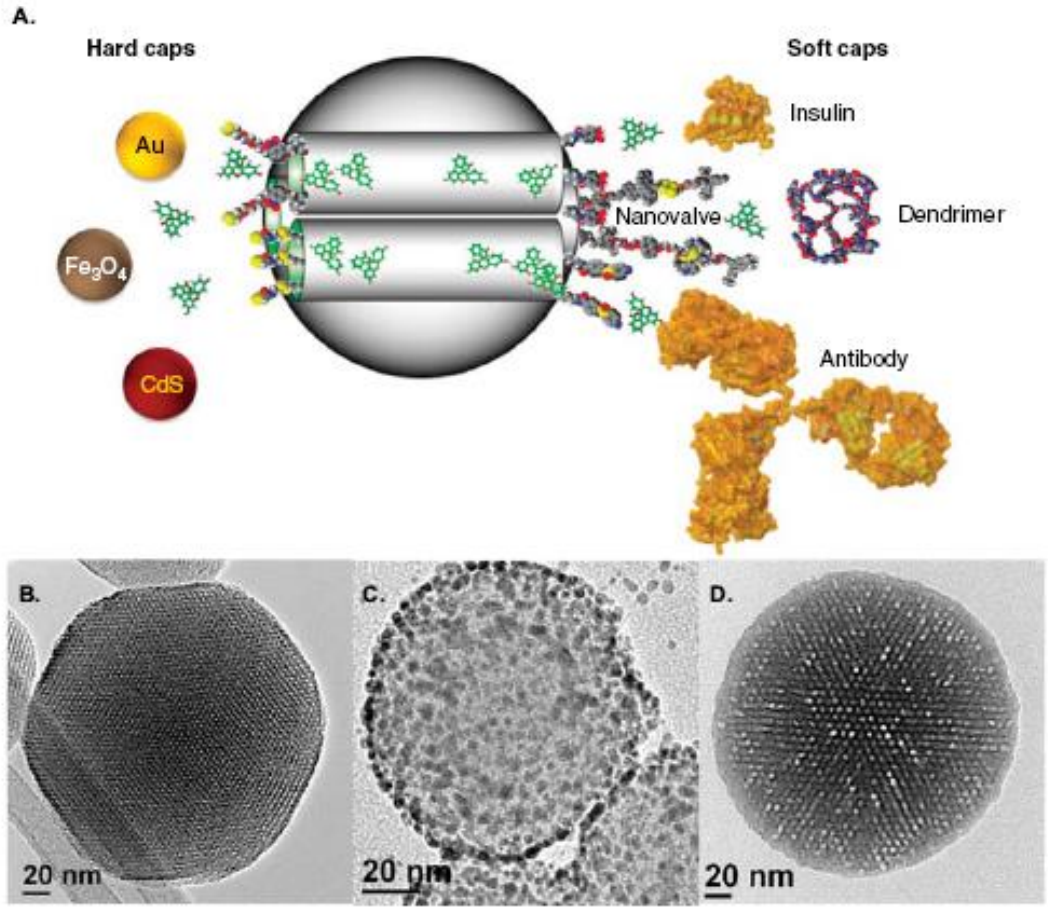

Figure 1. A. Schematic representation of a MSN loaded with drugs and capped with hard caps and soft caps highlighted in this review. Transmission electron microscopy images of (B) a MSN along the axis of the mesopores, (C) capped with hard (Au NP) and (D) with soft (polymer) caps.

MSN: Mesoporous silica nanoparticle.

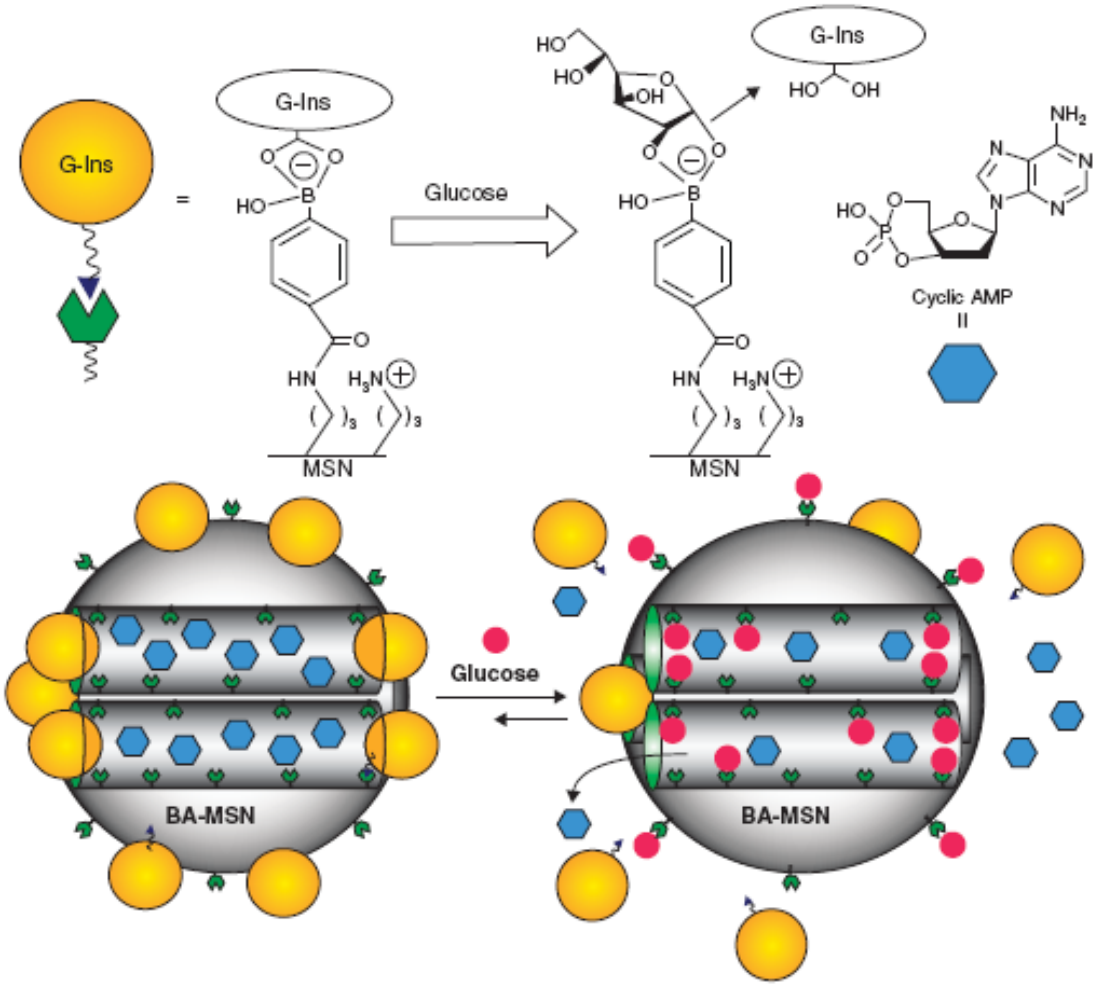

Figure 5. Schematic representation of the glucose-responsive MSN-based double delivery system for controlled release of bioactive G-Ins and cyclic AMP. The controlled release mechanism was achieved by means of the displacement reaction between blood glucose and G-Ins based on reversible boronic acid-diol complexation. High glucose concentration triggers the G-Ins uncapping and the release of cyclic AMP sequentially to diminish the higher than normal level of blood glucose.

Reproduced with permission from [19].

G-Ins: G-insulin; MSN: Mesoporous silica nanoparticle.

Polymer

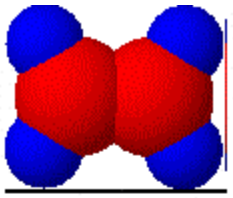

a monomer ethene

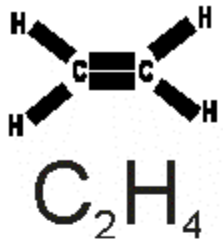

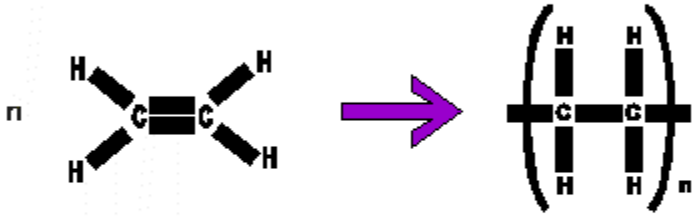

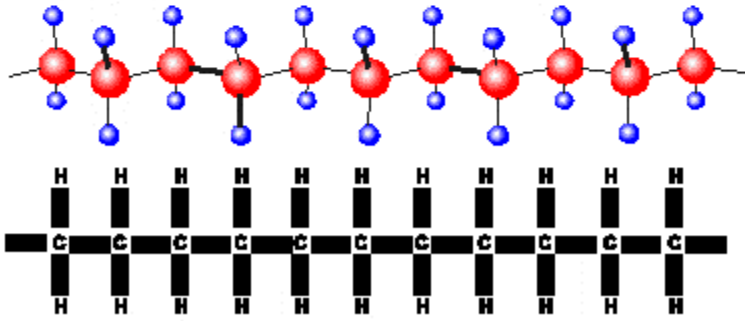

a polymer poly(ethene)

Block copolymer

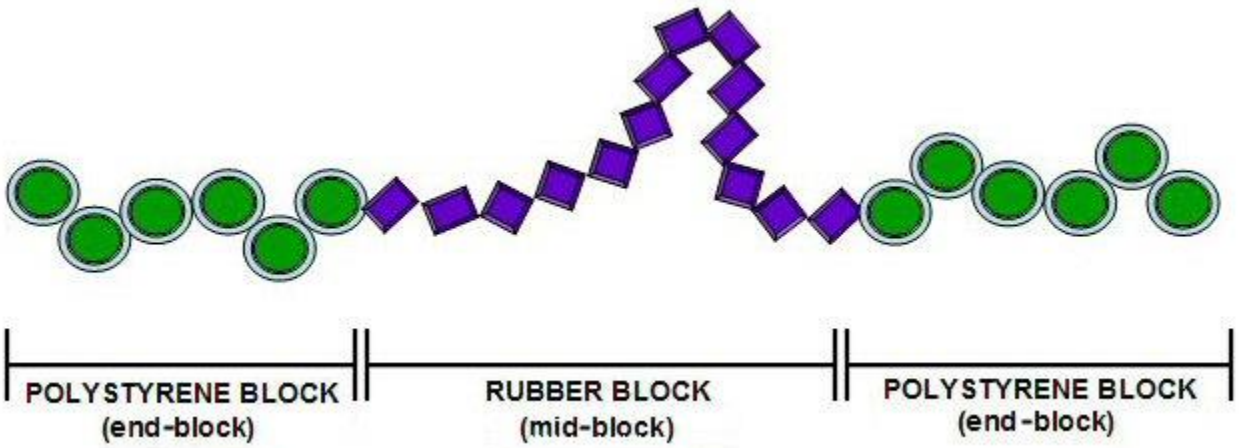

Phase Segregation

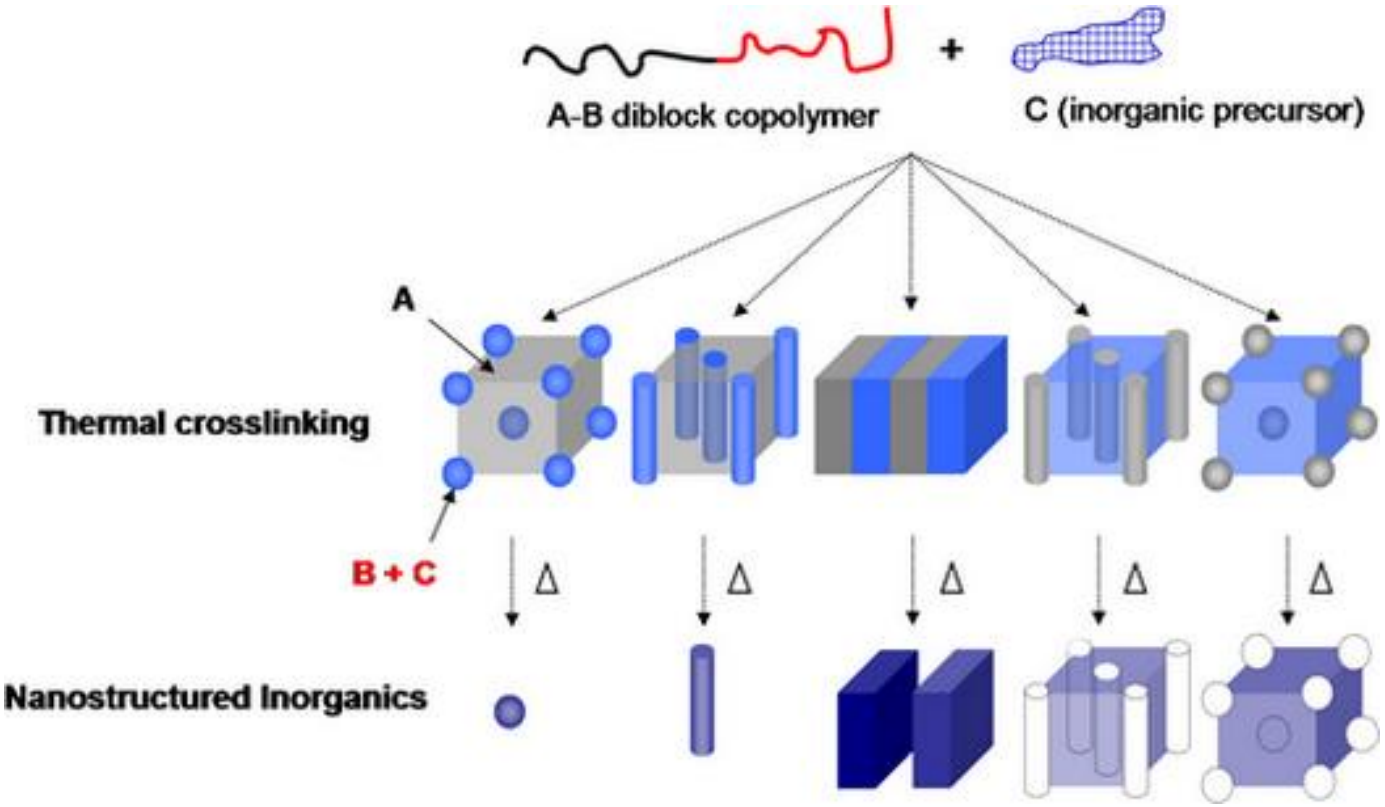

Self-Assembled Block-copolymer

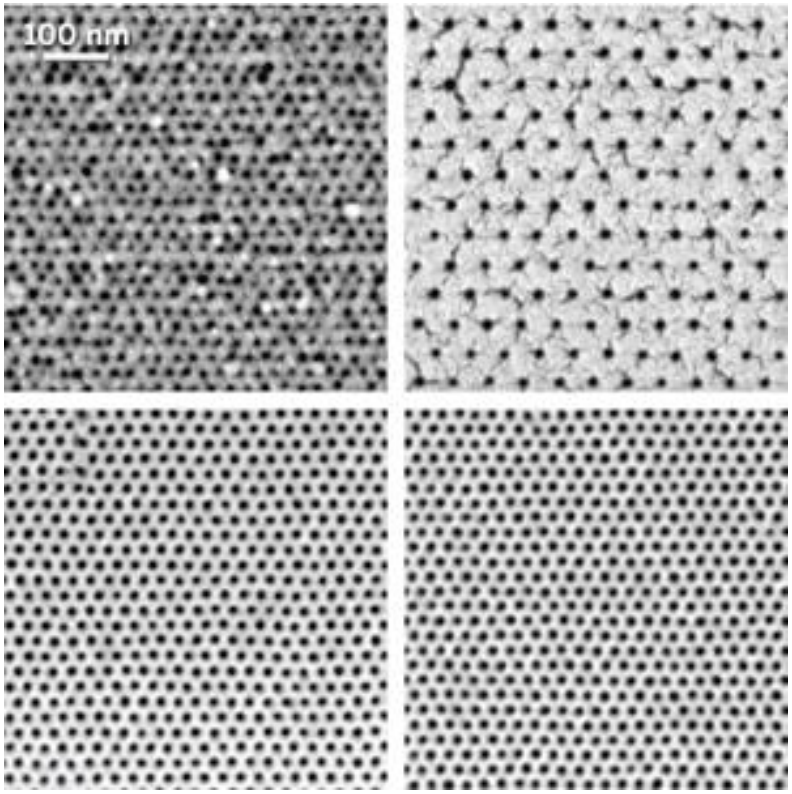

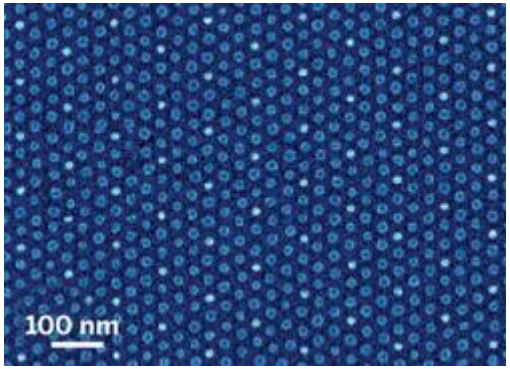

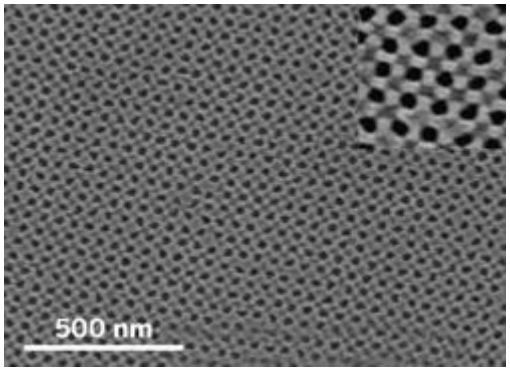

CNT

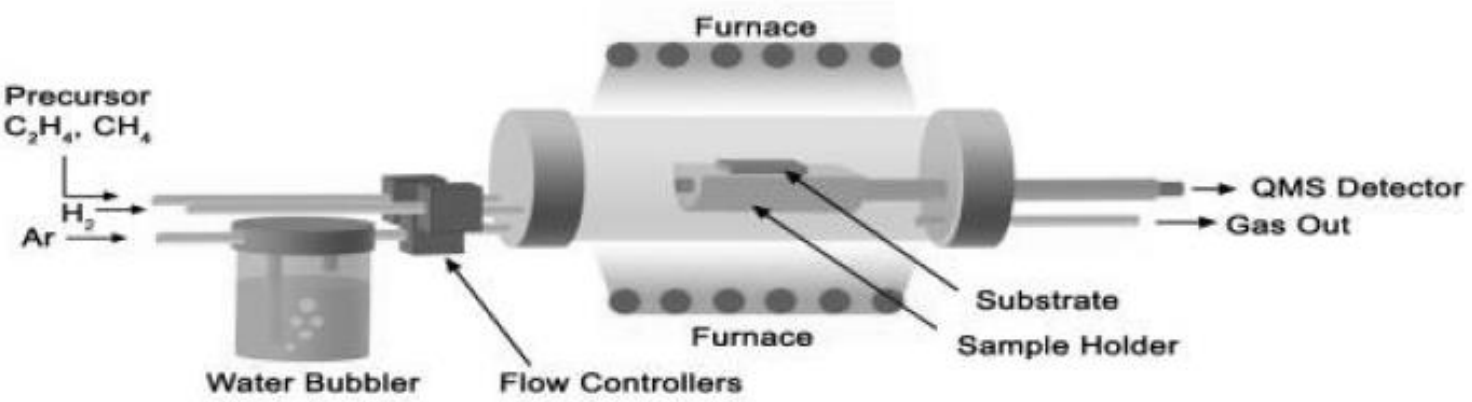

Fig. 1. Schematic of a CVD reactor for carbon nanotube growth. (Sketch by S. Yarmolenko from NCA&T State University)